Title:

Subsidence in Como historic centre (northern Italy): assessment of building vulnerability combining hydrogeological and stratigraphic features, Cosmo-SkyMed InSAR and damage data

Authors: Nicoletta Nappo [a], Dario Peduto [b,*], Marco Polcari [c], Franz Livio [a], Maria Francesca Ferrario [a], Valerio Comerci [d], Salvatore Stramondo [c], Alessandro Maria Michetti [a]

Affiliations

[a] Dipartimento di Scienza e Alta Tecnologia, Università degli Studi dell'Insubria, via Valleggio 11, 22100 Como, Italy

[b] Department of Civil Engineering, University of Salerno, via Giovanni Paolo II 132, 84084 Fisciano, Italy

[c] Istituto Nazionale di Geofisica e Vulcanologia (INGV), via di Vigna Murata 605, 00143 Rome, Italy

[d] Servizio Geologico d'Italia – ISPRA, via Vitaliano Brancati 48, 00143 Rome, Italy

*Corresponding author:
Department of Civil Engineering
University of Salerno (ITALY)
Via Giovanni Paolo II, 132 - 84084 - Fisciano (SA)
Office: +39089964120
Mobile: +393286935656

Keywords: subsidence, InSAR, hydrogeology, building damage, fragility curves, vulnerability

Highlights (max 85 characters – including spaces)

1) Areas with highest subsidence remarks pre-Roman lakeshore in Como city.
2) Building damage surveys reveal negligible to moderate severity levels.
3) Subsidence-related intensity parameters are derived from InSAR data.
4) Fragility curves for masonry/reinforced concrete buildings are derived.

Abstract

Como historic centre, located at the SW branch of Lake Como (northern Italy), is prone to subside because of a thick sequence of late Pleistocene to Holocene glacio-lacustrine, palustrine and alluvial sediments in the subsoil. After the 1950s, the combination of natural causes and anthropogenic activities amplified subsidence-induced differential settlements at building foundation depths, resulting in damage on the superstructures.

This work presents the first subsidence vulnerability analysis of the historic buildings in Como city centre by combining hydrogeological/stratigraphic properties, *in situ* damage investigations, and remote sensing Synthetic Aperture Radar (SAR) data acquired by Cosmo-SkyMed mission. First, the relationships between local hydrogeological features and vertical displacements retrieved by SAR Interferometry (InSAR) analysis were qualitatively assessed. This highlighted that cumulative vertical InSAR-derived settlements have a stronger linear correlation with the groundwater level rather than the thickness of compressible soil units at the city scale. The largest vertical displacements are located in the NW sector of the city centre and along the shore of Lake Como, where they remark the pre-Roman shoreline. Then, the cause-effect relationships between building damage severity and *Subsidence-Related Intensity* (SRI) parameters were investigated using a probabilistic approach based on empirical fragility curves. To this aim, two InSAR-derived SRI parameters were tested for both masonry and reinforced concrete buildings: differential settlements and relative rotations. The former resulted to relate better to distinct damage levels in Como historic centre. The analyses performed can contribute to the management of the inestimable architectural and cultural heritage of Como historic centre.

1. Introduction

The continuous ground lowering in subsiding areas can induce absolute and/or differential settlements at building foundation depth and, when the foundation cannot accommodate such movements, damage may occur on the superstructure [1-6]. The severity of building damage can be assessed using either analytical methods based on the beam theory to assess the global behaviour of a building [7], or empirical methods based on the analysis of a large number of samples (i.e. damaged buildings) in subsiding regions [5,8,9]. The encountered damage severity generally depends on *i)* intrinsic building features, i.e. geometry, number of floors, loadings, construction material, foundation typology, year of construction and (if applicable) maintenance status [10-12], and *ii)* intensity parameters specifically related to subsidence, e.g. absolute settlements, differential settlements, angular distortions and relative rotations [2,5,6,13]. Gathering information about the hydrogeological, stratigraphic and geotechnical setting where subsidence evolves is also essential to understand predisposing factors as well as its spatial evolution, thus obtaining reliable forecasting models of building vulnerability [11,14,15].

The vulnerability of buildings to natural hazards, such as subsidence, is often studied via fragility curves that allow assessing, for each building, its conditional probability of reaching or exceeding a specific damage severity level induced by a phenomenon of given intensity [10,11,15-19]. The intensity parameter associated to the phenomenon can be either physical or empirical [12].

The displacements related to subsidence phenomena are traditionally measured using GPS, geodetic levelling or borehole extensometers, which although being very valuable are expensive and difficult to be installed over wide regions [14,20]. In this perspective, Interferometric Synthetic Aperture

Radar (InSAR) techniques represent an effective alternative or complement to traditional instruments when investigating the spatial distribution and effects of subsidence over large areas [21,22]. The increasing number of space missions and the rapid development of sensors and processing algorithms allow InSAR to provide high quality measurements in the order of millimetres over a given period [15, 23-32]. Nowadays, InSAR-based ground displacement measurements and deformation time series are largely applied to investigate the effects of subsidence anywhere in the world, thus supporting the scientific community to improve the knowledge of such phenomena [e.g. 11,14,16,19,20,33-53].

This paper investigates the historic centre of Como municipality, which is located on the southwestern shore of Lake Como (northern Italy). This area is known to be affected by subsidence at a rate of few mm/year, mainly due to the presence of highly compressible unconsolidated Late Holocene organic clay and silty sediments, and its proximity to the lake that strongly influences the piezometric level [48,54-57]. Anthropogenic activities undertaken over the past 70 years (i.e. urban sprawl, deep aquifer exploitation between 1950 and 1975, and the construction of antiflooding facilities along the lakeshore in 2008-2010) altered the groundwater regime, thus amplifying the natural Holocene subsidence of the urban area up to 20 mm/year along the lakeshore and causing severe damage to several historic buildings of the city centre [48,54,55]. Since numerous cases of damaged buildings and infrastructure were reported in late 60s and early 70s, in 1974 the Como municipality established the technical commission “Commissione subsidenza” (i.e. Commission for subsidence) in order to investigate causes and effects of the ground settlements in Como urban area [58]. Based on levelling measurements from 1928 to 1979, hydromechanical information and the first damage survey in Como city dated 1975, the commission stated that i) the anthropogenic subsidence had a rapid development since the early 50s and then slowed down in 1975-1979 with velocities up to 10 mm/yr in few locations, and ii) the ground settlements were significant but almost homogeneous at the basin scale. Therefore, they could not establish any correlation between structural damage and subsidence at the single building scale [58].

In this paper, a large X-band SAR dataset acquired by Cosmo-SkyMed (CSK) mission of Italian Space Agency (ASI) from 2010 to 2019 was exploited to further investigate the subsidence phenomena occurring in Como municipality. In particular, as a novelty with respect to previous studies, the retrieved measurements were exploited to derive subsidence intensity parameters in order to perform the first vulnerability analysis for buildings of Como historic centre (called “città murata” and surrounded by Roman walls) using hydrogeological and stratigraphic data, and damage in-situ surveys. In particular, this paper aims at i) qualitatively assessing the relationships between the known drivers of subsidence and the ground settlements experienced by Como historic centre in 2010 - 2019, ii) investigating any correlation between subsidence and building damage by testing two different parameters describing the foundation movement, and iii) generating empirical fragility curves as a first attempt of vulnerability analysis at single building scale.

The main goal is contributing to a better understanding of the effects of subsidence on the historic buildings of Como city centre in order to preserve the local architectural heritage. Such vulnerability analyses are indeed fundamental for planning appropriate subsidence risk mitigation and prevention measures to avoid that a phenomenon with moderate intensity may turn into a disaster with unexpectedly severe consequences.

2. Study area and collected data

2.1 Hydrogeological, stratigraphic and geotechnical setting

The extensive work performed by several research groups in the past decades provided the current knowledge of Como basin. Specific interest was addressed to its geological framework and landscape evolution [59-63], hydrogeological setting [64,65], archaeology [66-69], active tectonics [70-72], post-Last Glacial Maximum evolution (Comerci, 2004; Comerci et al., 2007; Martinelli et al., 2019), hydrogeological [56] and geotechnical [54] models of the subsoil. Recently, the relationships between known subsidence drivers (i.e. the thickness of compressible soil layers and piezometric level) and ground movements derived from historical InSAR data from 1992 to 2010 have been investigated also by means of linear and nonlinear regression analyses [57].

The municipality of Como extends for about 37 km^2 at the SW end of the hydrologically closed branch of Lake Como in northern Italy (Fig. 1a). The urban area is built on an NW-SE oriented alluvial plain (Fig. 1b) drained by Cosia and Valduce streams, whose riverbed is currently culverted in the town underground. The plain is bordered by steep mountains composed of Mesozoic pelagic carbonates (Medolo Group – Early Jurassic) to the NE, and deep-sea fan conglomerates (Gonfolite Group – Oligo-Miocene) to the SW. The valley floor conceals the trace of a regional backthrust (Gonfolite backthrust; Fig. 1b) [70,75]. During the Quaternary, the morphology of the basin was repeatedly shaped by the erosional and depositional activity of glaciers [59,76-78], thus determining a high heterogeneity in the lithostratigraphic and geotechnical setting (Fig. 1c) [54,56].

The stratigraphy of Como historic city centre was retrieved from the database acquired directly by University of Insubria or collected from Como Municipality and/or other companies [54-56]. From the surface level up to a maximum depth of 180 m, the Como sedimentary sequence is composed as follows (Fig. 1d): i) heterogeneous reworked materials with archaeological remains up to a maximum depth of 10 m in the lakeshore area (Unit 1 - RM) and decreasing thickness up to 3 m in the remaining urban area; ii) alluvial sands and gravels up to 15-24 m (Unit 2 - SG); iii) palustrine organic and highly compressible silts up to 30 m (Unit 3 - OS) with sandy (Unit 3a) or clayey facies (Unit 3b) that reach their maximum thickness approximately in the centre of the basin and gradually decrease up to 2 m at margins; iv) glaciolacustrine sediments with dropstones up to 40-60 m (Unit 4 - SD) and v) coarser proximal deposits up to 80-100 m (Unit 5 - CD) with spatial distribution similar to Unit 3 - OS. In the lakeshore area, silty and highly compressible sub-units within anthropogenic sediments were also recognized [56].

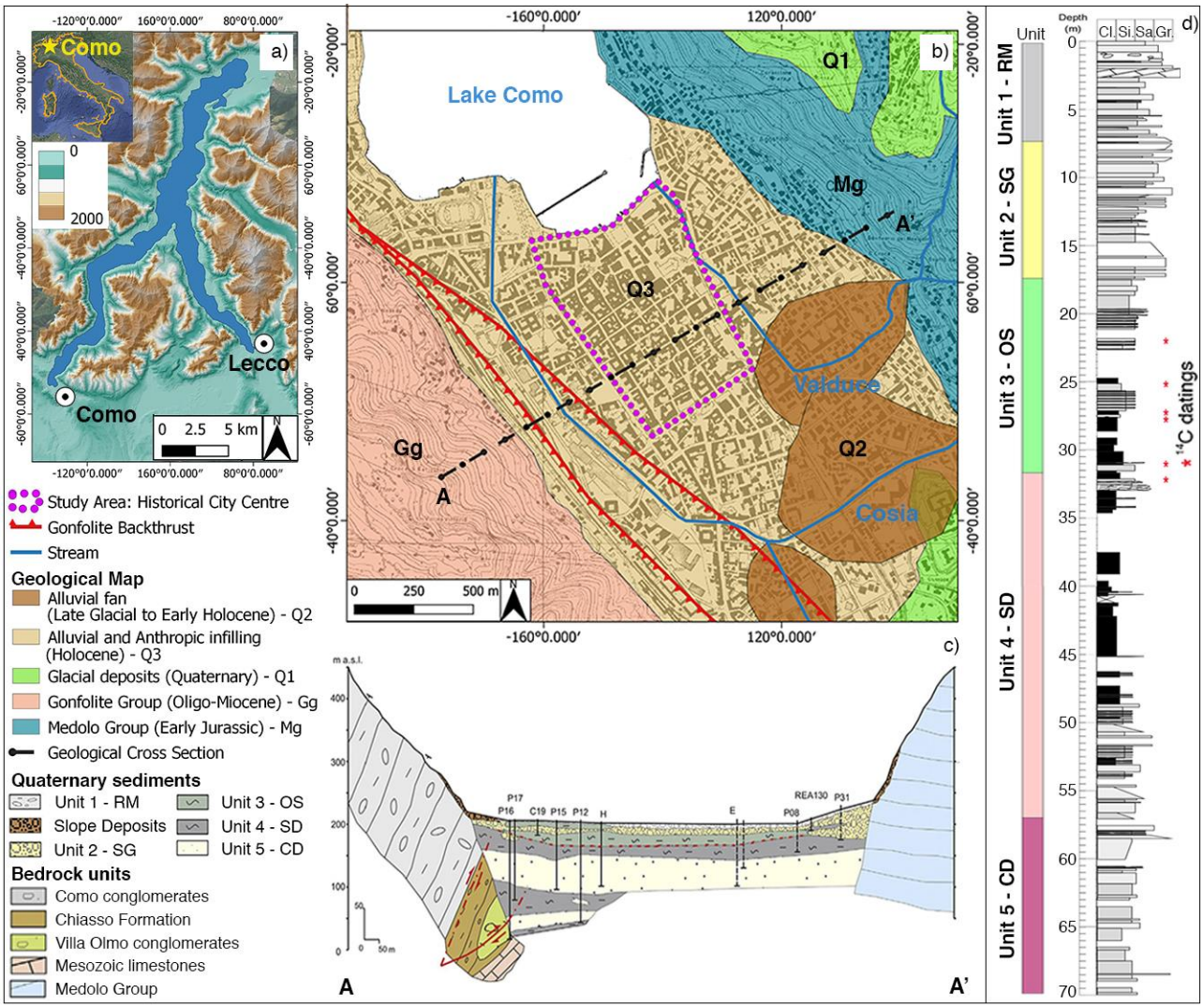

Figure 1. Modified from Nappo et al. [57]. Reference system: WGS84/UTM zone 32N. a) Location of Como municipality with respect to the Lake Como. b) Simplified geological map of the hydrologically-closed Como basin (modified after Servizio Geologico d'Italia [78]) filled with fine grained compressible late Pleistocene to Holocene lacustrine to palustrine sediments. c) Geological cross section of the basin (modified after Ferrario et al. [56]); note the Gonfolite backthrust at the base of the Oligo-Miocene Gonfolite Group. d) Example of borehole profile in Como historic centre with Cl (clay), Sl (silts), Sa (sand) and Gr (gravel) particles (modified after Ferrario et al. [56]); according to extensive radiocarbon dating this stratigraphic column spans the last ca. 20 kyr, that is the post-LGM time window (Ferrario et al. [56]).

The geotechnical properties of Como basin are known thanks to in-situ Standard Penetration Tests (SPT), Lefranc Permeability Tests (LPT), Cone Penetration Tests (CPT) and laboratory tests performed by different research groups [e.g. 54-56]. For the reader's convenience, Table 1 summarises the geomechanical parameters of the sedimentary sequence of the basin.

Table 1. Geomechanical parameters of stratigraphic units in Como subsurface (modified after Ferrario et al. **[56]**).

	Unit 1 - RM	**Unit 2 - SG**	**Unit 3 - OS**	**Unit 4 - SD**	**Unit 5 - CD**
N-value (SPT)	5 – 30	> 100			40 – 50
Tip resistance [kPa]			40 – 150		
Cone resistance (Qc) [mPa]	1 - 10	1 - 10	1.6 – 2.4		
Unit weight [kN/m^3]	19.0	19.0	18.0	18.0	20.0
Permeability coefficient (k) [m/s]	10^{-5} – 10^{-6}	10^{-2} – 10^{-8}	10^{-6} – 10^{-8}	10^{-6} – 10^{-9}	
Friction angle [°]	34	34	24	24	32
Cohesion (c') [kPa]	0	0	0	0	0
Undrained cohesion (cu) [kPa]	0	0	50	50	0
Young Modulus (E) [kPa]	12 - 15	12 – 15			
Confined Modulus (Mo) [kPa]			1.6 – 2.6 (depth 15-40 m)	3.7 – 4.0 (depth 40-55 m)	

The stratigraphy and geotechnical properties were retrieved from 261 borehole logs (Fig. 2a) acquired during drilling campaigns at different depths for public and private projects (e.g. building construction, water extraction, restoration of the Como lakefront).

The municipal piezometric network nowadays counts 28 active piezometers (Fig. 2b) that measure the depth of the phreatic water table in Como municipality. However, the limited availability of recent piezometric records (i.e. later than 2015) did not allow extrapolating up-to-date information about the phreatic level in Como city centre. Therefore, as previously done by Ferrario et al. [56], Bajni et al. [54] and Nappo et al. [57], the isopiezometric curves representing the mean level of surficial aquifer of Como basin [58] were adopted in this paper as piezometric indicator. In absence of anthropic disturbances, seasonal fluctuations of the piezometric level vary from about 1.5 m near the lakeshore to 0.5 m moving towards the SE part of the basin [54-56].

The thickness of Unit 1 – RM and Unit 3 – OS, together with the average piezometric level of the phreatic aquifer, have already been proved the principal drivers of subsidence in Como area [e.g. 54-57].

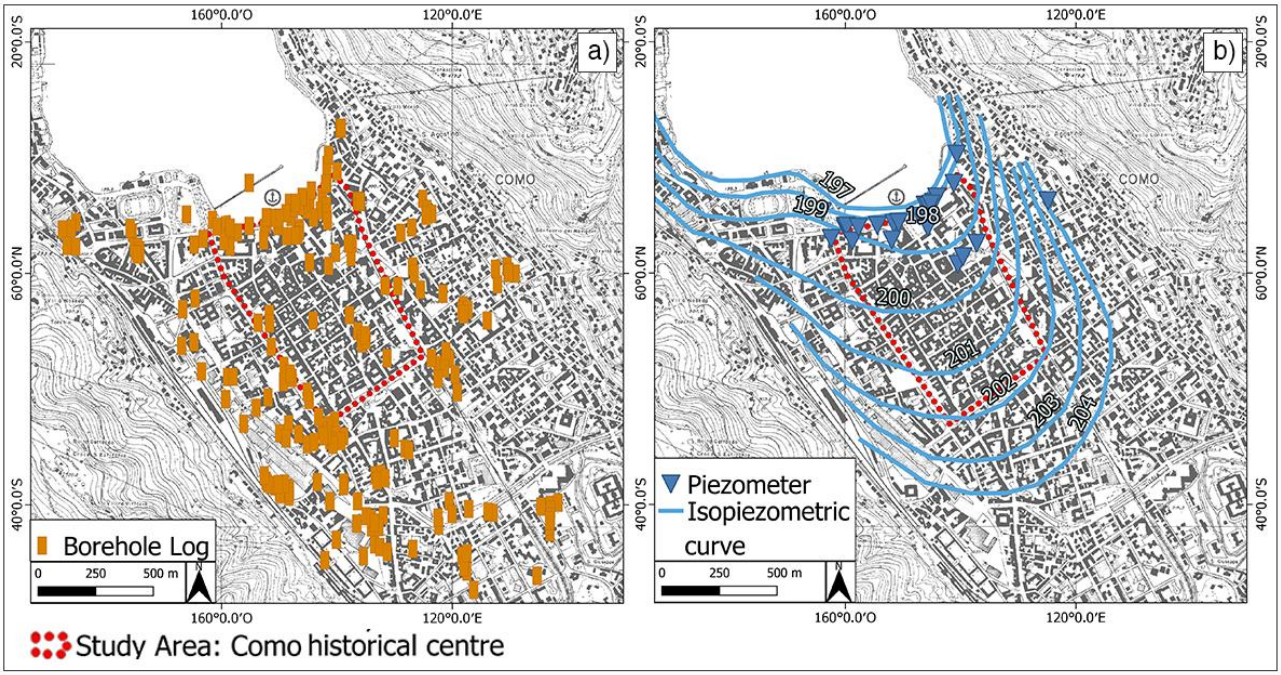

Figure 2. Reference system: WGS84/UTM zone 32N. a) Borehole logs as collected by University of Insubria (modified from Ferrario et al. [56] and Nappo et al. [57]). b) Municipal piezometer network and isopiezometric curves (modified after Comune di Como [58]; Ferrario et al. [56] and Bajni et al. [54]).

2.2 InSAR data

A stack of 167 X-band Single Look Complex (SLC) SAR images acquired in Strip-map mode by CSK mission of ASI from June 2010 to July 2019 along descending track was collected in order to investigate any ground subsidence phenomena in the historic centre of Como municipality. The InSAR analysis was performed by the multi-baseline Interferometric Point Target Analysis (IPTA) approach developed in the framework of GAMMA software [79,80]. First, multi-look factors of 5 by 5 was applied to reduce the speckle noise, thus obtaining the same pixel spacing of the ~10m TINITALY Digital Elevation Model (DEM; http://tinitaly.pi.ingv.it/) exploited to remove the topography from the interferometric phase. All the interferometric pairs characterized by a maximum perpendicular baseline of 350 m and a maximum time span of 500 days were estimated returning a dense network consisting of more than 1300 interferograms (Fig. 3a). Then, the data were filtered by applying the Goldstein filtering with a window size of 8 pixel and an exponent of 0.4 [81] and unwrapped by the minimum cost flow algorithm with coherence threshold set to 0.4 [82]. The interferograms characterized by large atmospheric artefacts or unwrapping errors were discarded. Therefore, the point targets candidates were selected with coherence threshold approach by setting the minimum coherence to 0.4 for acceptable targets. The estimated interferograms were then sampled by using the selected point targets maps, and the final solution was estimated by Singular Value Decomposition (SVD) analysis.

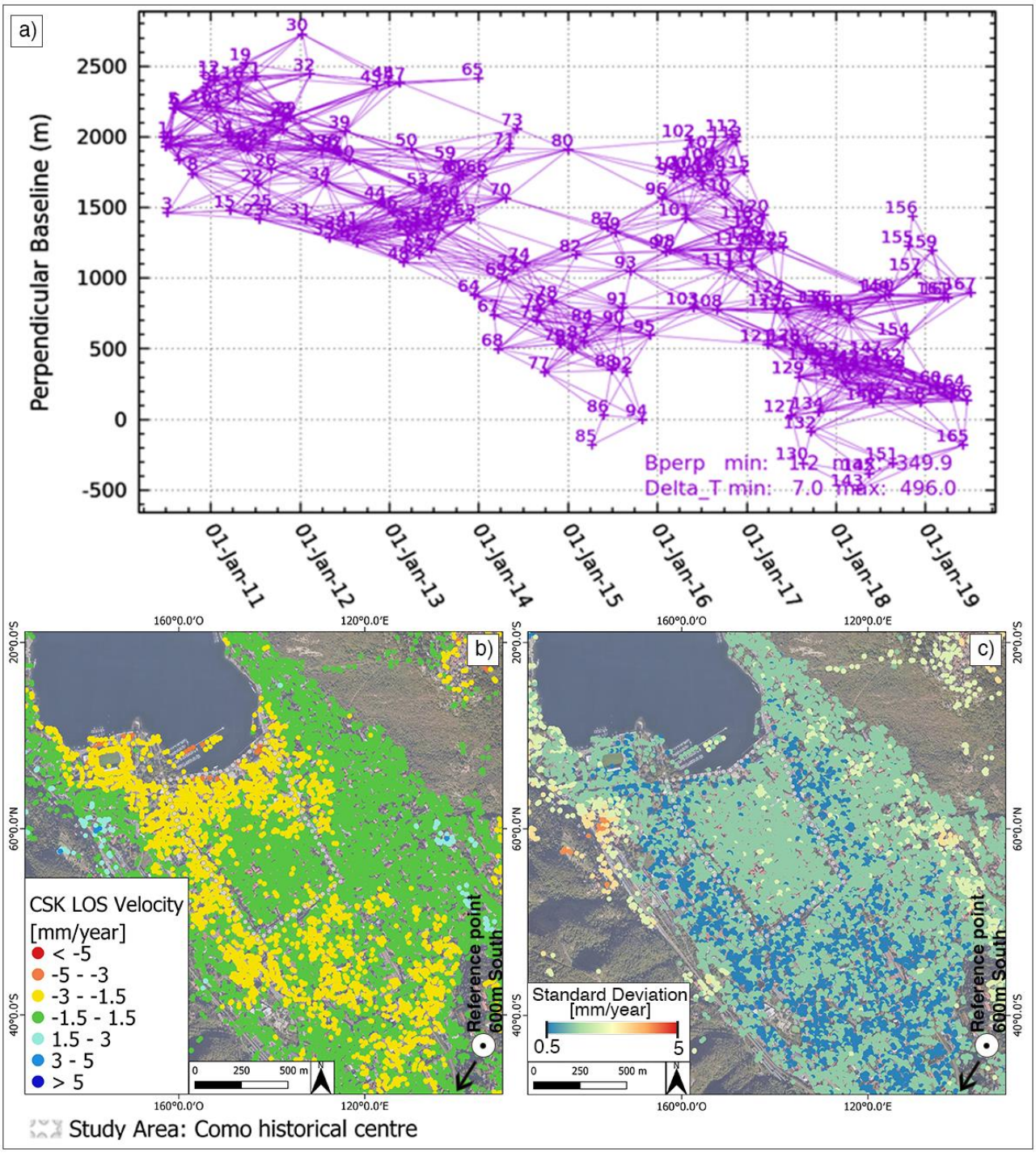

Figure 3. Reference system: WGS84/UTM zone 32N. a) Interferogram network of more than 1300 interferograms. Multi-baseline IPTA results from Cosmo-SkyMed (CSK) InSAR data: b) LOS velocity and c) standard deviation.

The output of the processing phase is a set of sparse point targets (PT hereafter; Fig. 3b) with the following attributes: PT identifier, geographic coordinates, coherence, mean annual velocity along the Line of Sight (LOS), standard deviation, and displacement time series. These InSAR measurements are temporally dependant on the first acquired image, and spatially relative to a reference point located on the bedrock site of Camerlata (in the south part of Como municipality) and supposed to be stable [55]. Figure 3c shows the distribution of PT standard deviation.

2.3 Building features

To obtain information about the characteristics, distribution and severity of damage on buildings in Como historic centre, 600 buildings were identified from the topographic map (Carta Tecnica Regionale – CTR, at 1:10.000 scale [83]), and their geometric and structural information (i.e. volume, number of floors, construction material and year of construction) collected from the Como Municipality repository [84] (e.g. Fig. 4). The investigated buildings are mainly of masonry type (528 out of 600), with some reinforced concrete (57 out of 600) and few in stones (15 out of 600). Unfortunately, information on the typology of foundation was not available. Therefore, knowing the period of construction and typical practise in the area, for the purpose of the present study all buildings were assumed as resting on shallow foundations with typical depth smaller than 4 m. Accordingly, the buildings are likely to be founded on the Unit 1 – RM.

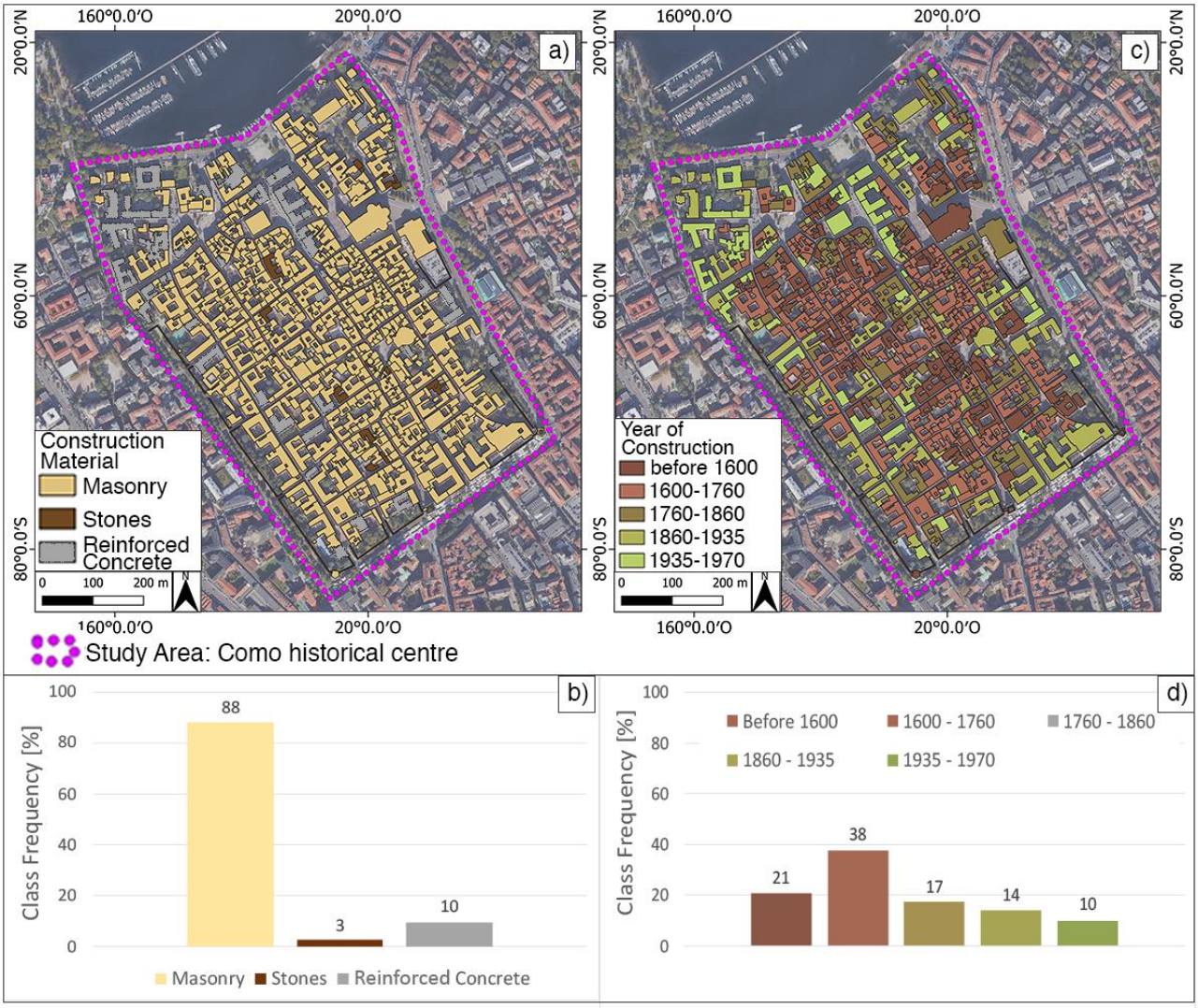

Figure 4. Reference system: WGS84/UTM zone 32N. Classification of the 600 surveyed buildings according to their a) - b) construction material, and c) - d) year of construction.

3. Methodology

The procedure followed in this study consists of two phases, as summarised in Figure 5. In *Phase I*, the relationship between main drivers of subsidence (i.e. thickness of Unit 1 – RM and Unit 3 – OS,

and piezometric level) and ground surface displacements in Como urban area were qualitatively investigated for years 2010-2019. In *Phase II*, the relationship between ground settlements and building damage was determined by testing two InSAR-derived *Subsidence-Related Intensity* (SRI) parameters [11,15], and then empirical fragility curves describing the vulnerability of the city centre were generated.

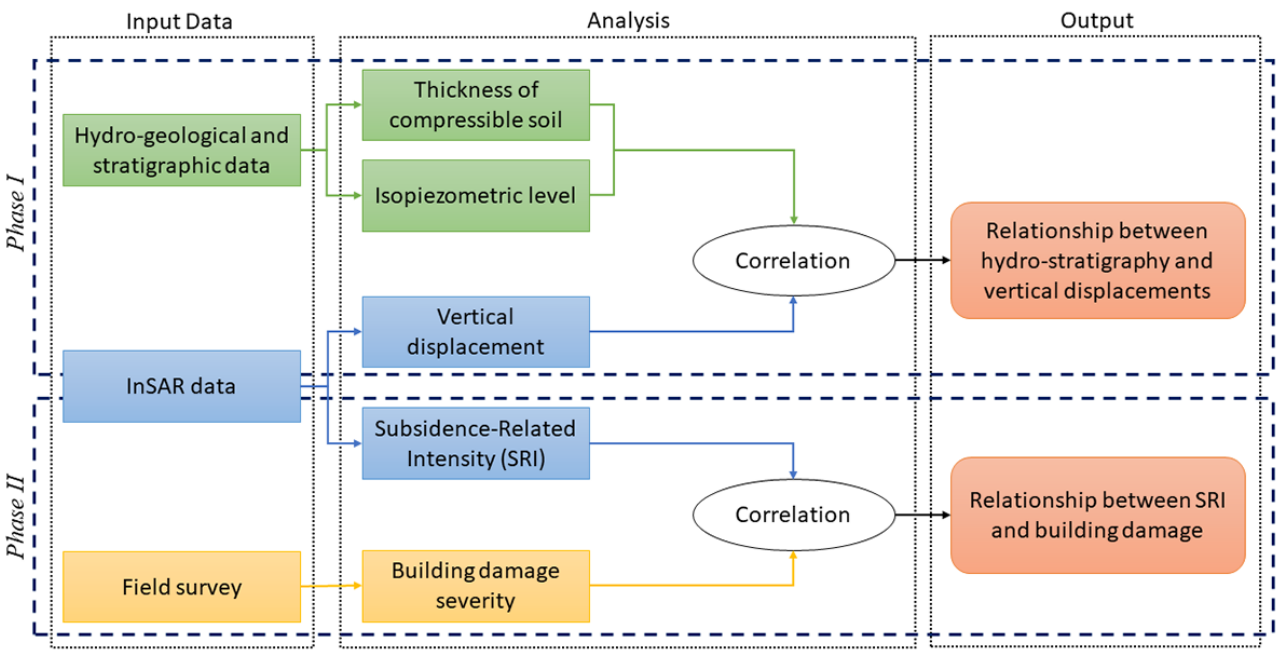

Figure 5. Schematic flowchart of adopted methodology.

As preliminary step, the cumulative displacement (δ_{cum}) of each PT along the LOS direction was calculated as the difference between the last and the first measures (δ_{last} and δ_{first}, respectively) of its time series:

$$\textbf{(1)} \quad \boldsymbol{\delta_{cum} = \delta_{last} - \delta_{first}}$$

This allows to consider different distributions of the displacement rate over time, rather than linear. Then, considering vertical movements predominant in the flat subsiding area of Como basin, the vertical component of the cumulative displacement (δ_{vert}) of each PT was calculated as proposed in Cascini et al. [37]:

$$\textbf{(2)} \quad \boldsymbol{\delta_{vert} = \delta_{cum} / \cos\vartheta}$$

where ϑ is the CSK incidence angle, equal to about 26°.

Once all data were collected, in *Phase I* the hydrogeological data (i.e. thickness of Unit 1 – RM and Unit 3 – OS) were interpolated via Empirical Bayesian Kriging (EBK), and the InSAR δ_{vert} with Ordinary Kriging. For both interpolations the spatial resolution was set to 10x10m to be coherent with the final ground resolution obtained for InSAR data. Different interpolation methods were necessary to take into consideration the density and spatial anisotropy of each dataset. The sparse and heterogeneous boreholes data (Fig. 2a) were modelled via EBK with a power semivariogram type

that allows to statistically predict the values of sampling points where lacking [85]. InSAR data are instead homogeneously spaced (Fig. 3b), therefore Ordinary Kriging [86] modelled with spherical semivariogram type better smooths the high variability of their values. As for the piezometric data, the isopiezometric curves (Fig. 2b) were rasterized with a grid of 10x10m to be comparable with other measurements. Then, the (linear) correlation between interpolated hydrogeological features and InSAR δ_{vert} was assessed using the Pearson's Correlation Coefficient (PCC). The existing correlation can be classified as *null* when PCC < |0.25|, *weak* for |0.25|< PCC < |0.50|, *moderately strong* when |0.50|< PCC < |0.75|, and *strong* for |0.75|< PCC < |1|. Finally, the interpolated data were plotted along two cross sections of the study area to qualitatively assess the local relationships between hydrogeological features and InSAR δ_{vert}.

In *Phase II*, knowing that damage on superstructures can occur when the building foundation cannot accommodate differential settlements or relative rotations [e.g. 5,11,13,15,34,35], both parameters were derived. To this end, a 2-meter buffer was preliminary drawn around each building to consider the geo-localization errors of InSAR point targets (PT) and topographic map projections. For each 2-meter-buffered building (e.g. Fig.6), the PT exhibiting the maximum and the minimum vertical displacement ($\delta_{v,max}$ and $\delta_{v,min}$, respectively) were determined together with their distance (L). Then, the differential settlements (Δ) and relative rotation (θ) were computed as follows [e.g. 9,15,49]:

$$\Delta = \left|\delta_{v,max} - \delta_{v,min}\right| \quad (3)$$

and

$$\theta = \Delta / L \quad (4)$$

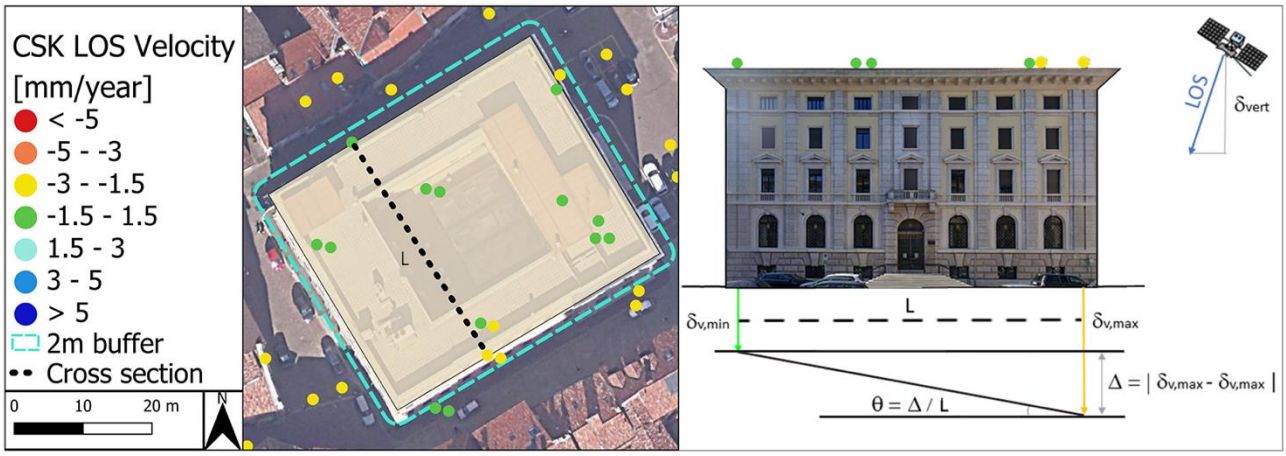

Figure 6. Reference system: WGS84/UTM zone 32N. Scheme of SRI calculation for a sample masonry building in Como city centre.

Importantly, in the present study, PT-measured settlements were assumed as occurring at the foundation depth, thus disregarding both compressive and tensile strain that may affect the superstructure [15].

Both differential settlements (Δ) and relative rotation (θ) were used as descriptors of *Subsidence-Related Intensity* (SRI) and correlated with the damage severity [11,15] in order to assess the most suitable parameter.

As for the ranking of damage, the classification of severity was adapted from Burland et al. [4], who distinguished the damage degrees based on the approximate crack width (w) and the easy of repair

as: negligible (w < 0.1 mm); very slight (w < 1 mm); slight (w < 5 mm); and moderate (w > 5 mm). Hereafter, these damage severity levels are labelled from D1 to D4 (Fig.7).

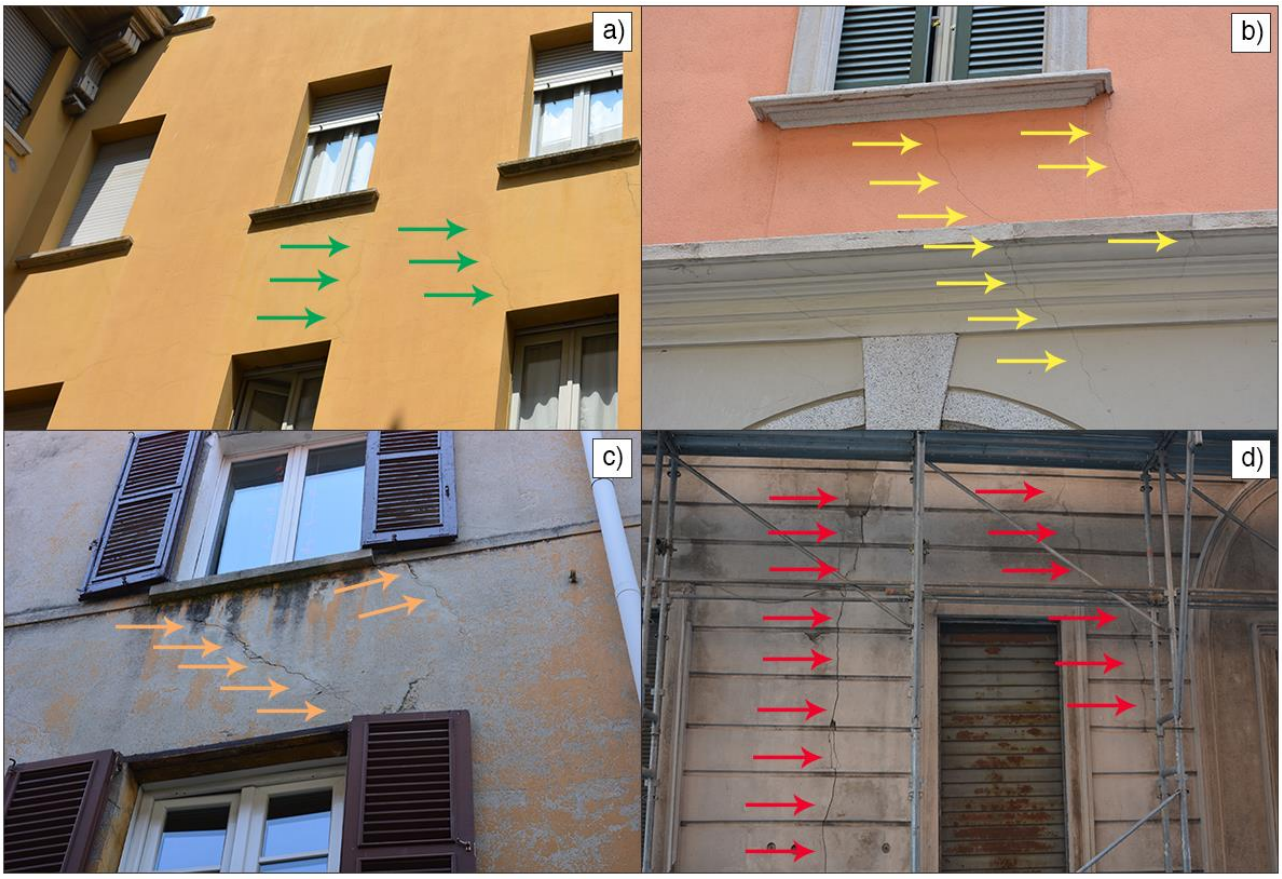

Figure 7. Building damage severity levels (modified from Burland et al. [4]): a) D1 (negligible, w < 0.1 mm); b) D2 (very slight, w < 1 mm); c) D3 (slight, w < 5 mm); d) D4 (moderate, w > 5 mm). Photos taken on 3-14 June 2019.

Subsequently, the conditional probability for a building to reach or exceed a certain damage severity level for a given SRI value was calculated via fragility curves [10-13,15,17-19] as:

$$(5) \qquad P\,(Damage \geq D_i) = \Phi\left[\frac{1}{\beta}\, ln\left(\frac{SRI}{\overline{SRI}}\right)\right]$$

where D_i (for i = 1, 2, 3, 4) is the damage severity level, Φ is the standard normal cumulative distribution function, β is the standard deviation of natural logarithm of SRI for each D_i, and $\overline{SRI}$ is the median value of SRI associated to each D_i.

4. Results

4.1 Phase I – Hydrogeology, stratigraphy and InSAR vertical displacements

As for the qualitative assessment of the relationship between hydrogeological data and InSAR-derived vertical displacements (δ_{vert}), Figure 8 shows the interpolated and rasterized dataset for Como historic centre with 10x10m grid spacing. Interestingly, the largest vertical displacements are registered in the lakefront area and along the western border of the historic city centre, as following

the trace of the ancient Lake Como coastline (approximately I century BC) [67,73] before Romans established in the area and reclaimed land to found Como city (59 BC).

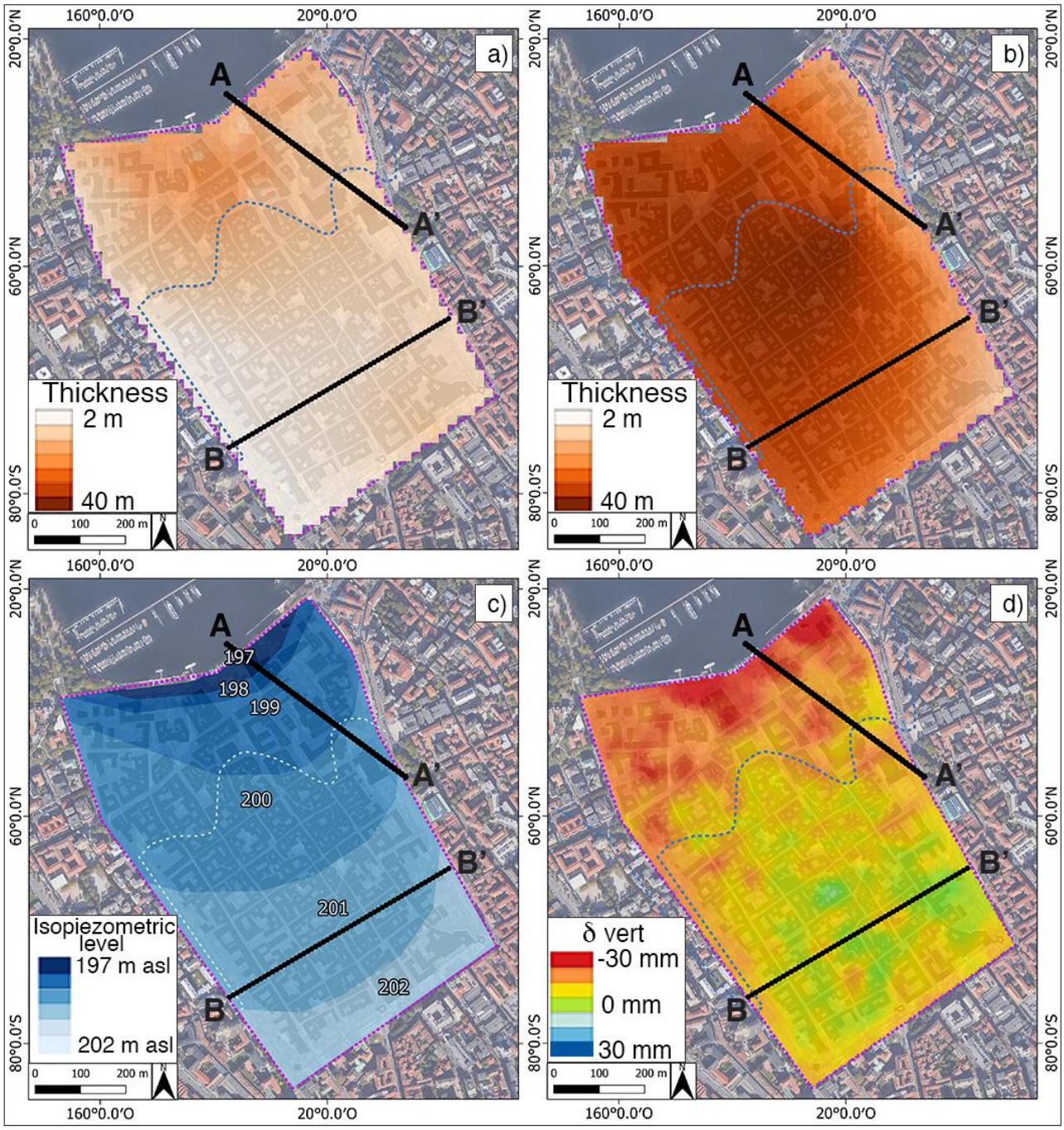

Figure 8. Reference system: WGS84/UTM zone 32N. Interpolation of a) thickness of Unit 1 – RM, and b) thickness of Unit 3 – OS via EBK. c) piezometric level obtained by rasterizing the isopiezometric curves (modified from Ferrario et al. [56]). d) Interpolation of InSAR cumulative vertical displacement (δ_{vert}) via Ordinary Kriging. The blue dashed line represents the ancient Lake Como coastline (dated about I century BC), and the black dotted lines two cross sections known from Ferrario et al. [56]).

The Pearson's Correlation Coefficient ($PCC = Covariance_{(hydrostratigraphy,\delta_{vert})} / \sigma_{hydrostratigraphy} \cdot \sigma_{\delta_{vert}}$) computed over the entire city centre showed that the δ_{vert} has a moderately strong linear correlation with the piezometric level and the area interested by the pre-Roman lake, followed by the thickness of Unit 1 - RM (Tab. 2). The thickness of Unit 3 – OS is

instead not-linearly related to δ_{vert}. These results were then compared with the relationships obtained in Nappo et al. [57] between the hydrogeological variables and the InSAR-derived vertical displacements retrieved from two additional sensors (i.e. ERS 1&2 and Envisat of the European Space Agency) for years between 1992 and 2010 (Tab.2). From the comparison emerges that over a time period of about 30 years only the piezometric level shows a constant linear correlation trend, while other stratigraphic factors are almost constant only in the last two decades.

Table 2. Results of Pearson's Correlation Coefficient (PCC) analysis and comparison with Nappo et al. [57].

		ERS 1&2 (1992-2000)*		Envisat (2003-2010)*		CSK (2010-2019)	
		PCC and type of correlation		PCC and type of correlation		PCC and type of correlation	
δ_{vert} vs	Thickness Unit 1 - RM	-0.46	Weak	-0.63	Moderately strong	-0.66	Moderately strong
	Thickness Unit 3 - OS	-0.56	Moderately strong	-0.21	Null	-0.13	Null
	Piezometric level	0.76	Moderately strong	0.74	Moderately strong	0.73	Moderately strong
	Pre-Roman lake					-0.74	Moderately strong

*These results are modified from Nappo et al. [57]

Then, as shown in Figure 9, the interpolated data were plotted along two cross sections (black dotted lines in Figure 8) for which the stratigraphy is known from Ferrario et al. [56]. The cross section AA' (Figs. 9a-d) shows an overall linear relationship between hydrogeological variables and InSAR-derived displacements, with a detrending moving from NW to SE of the historic centre. Here, the thickness of Unit 1 – RM varies from 9 to 4 m along the section (Fig. 9a), whereas that of Unit 3 - OS from 25 to 11 m (Fig. 9b); the piezometric level passes from 197 to 201 m asl (Fig. 9c) and the δ_{vert} ranges between -30 and -15 mm (Fig. 9d). The lakefront area is subjected to seasonal variations of the piezometric level. Although the recent construction of fixed and movable bulkheads, detention tanks and jet grouting barriers along the lakefront as antiflooding facilities altered the groundwater regime in this area, the natural piezometric level was re-established in 2010 [54].

As for the cross section BB' (Figs. 9 e-h), the largest vertical displacements ($\delta_{\mathrm{vert}} \cong -16$ mm) are concentrated at the SW side of the city centre with an overall decreasing trend towards NE (Fig. 9h). Along this section, the thickness of Unit 1 – RM (Fig. 9e) varies from 2 to 4 m, whereas that of Unit 3 – OS (Fig. 9f) progressively decreases from 30 to 10 m. The piezometric level is constant at 201 m asl along the section, with a slight variation of 1 m asl at the NE border (Fig. 9g). The δ_{vert} (Fig. 9h) shows higher variability along the section, with a difference in the range of 10 mm between minimum and maximum peaks.

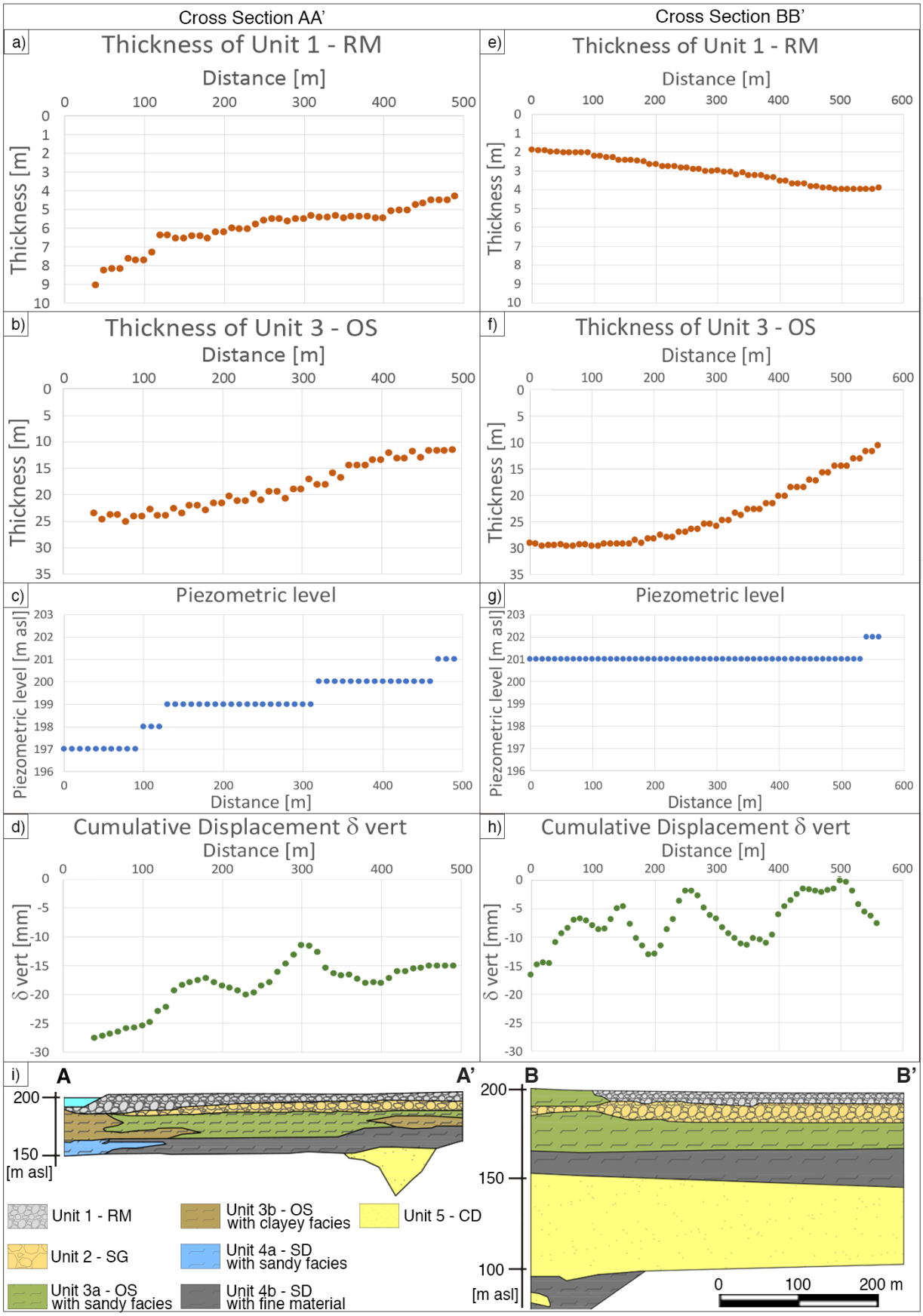

Figure 9. Profiles of a) thickness of Unit 1 – RM, b) thickness of Unit 3 – OS, c) piezometric level and d) InSAR δ_{vert} along the AA' cross section. Profiles of e) thickness of Unit 1 – RM, f) thickness of Unit 3 – OS, g) piezometric level and h) InSAR δ_{vert} along the BB' cross section. i) Geological cross sections (modified after Ferrario et al. **[56]**); the traces of both cross sections are shown in Figure **8**.

4.2 Phase II – SRI and fragility curves

In-situ investigations in Como historic centre were carried out in June 2019 to assess the crack patterns (i.e. location and orientation of cracks on the façade) and measure the average width of cracks for each building. The overall information gathered for the 600 surveyed buildings were summarised in fact-sheets as shown in Figure 10, where each building is classified according to the damage severity levels previously described.

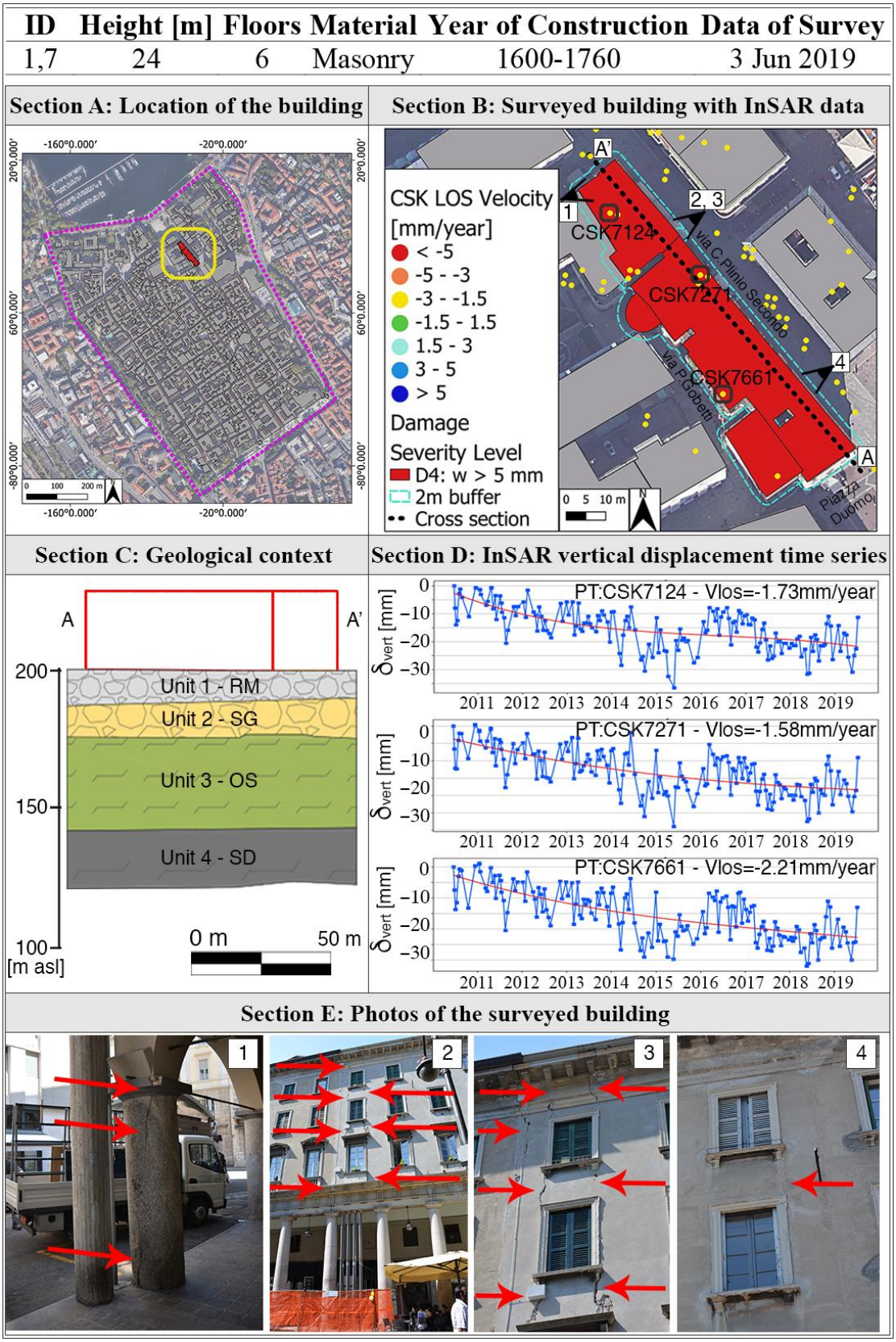

Figure 10. Reference system: WGS84/UTM zone 32N. Example of building data collection (modified after Peduto et al. [11]). Section A: Location of the building in Como city centre. Section B: Close-up view of the surveyed building with InSAR data. Section C: Simplified cross section of the surveyed building and the underlying stratigraphic units along the section shown in Section B. Section D: InSAR vertical displacement time series (δ_{vert}) of some PTs located on the surveyed building and framed with the black squares in Section B. Section E: Photos of the surveyed building taken on 3-14 June 2019; the pictures' points of view are reported in Section B.

Once the damage survey was completed and all information stored in the fact-sheets, a damage severity map (Fig. 11a) was retrieved for Como historic centre. The majority of the surveyed buildings (394 out of 600, i.e. 66%) resulted to be damaged. When no cracks were observed on structures' façades, these were classified as "No Damage" encompassing either not-affected buildings or recently maintained ones. Among the damaged buildings, the most frequent damage severity classes are D3 (42%) and D2 (31%), followed by D4 (20%) and D1 (7%) as shown in Figure 11b. When overlaid with InSAR PT map, the 600 surveyed buildings were classified also according to their differential displacement (Δ), as shown in Figure 11c. Not negligible Δ values (i.e. Δ≠0) were computed for 449 out of 600 buildings (i.e. 75%), the majority (36%) of which presented displacements ranging between 5 and 10 mm.

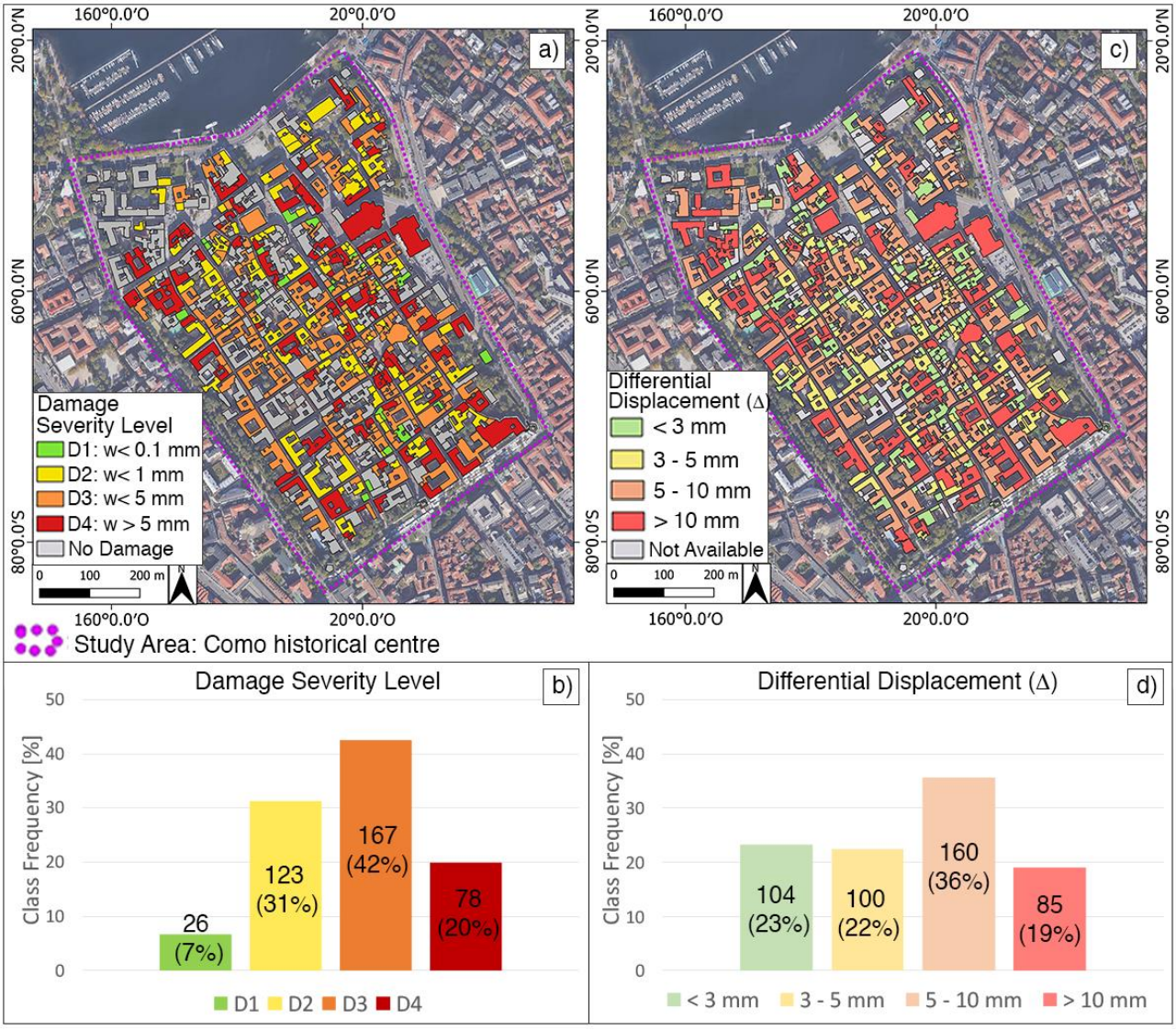

Figure 11. Reference system: WGS84/UTM zone 32N. a) Damage severity map of Como historic centre. b) Distribution of severity levels for 394 damaged buildings. c) Map of buildings with InSAR-derived differential settlement Δ. D) Histogram of 449 buildings with not-negligible Δ.

Table 3 summarises the number of buildings with i) non-negligible damage (i.e. severity level ≠ No Damage), ii) non-negligible differential displacements (i.e. Δ≠0), and iii) the intersection of both

samples, distinguished according to their construction material. To proceed with the subsequent steps of the analysis, only buildings with both non-negligible damage and Δ were considered. However, buildings constructed in stones were discarded because of their limited number (Tab. 3), which resulted not sufficient to construct the empirical fragility curves.

Table 3. Number of buildings with i) damage severity level ≠ No Damage, ii) differential displacement Δ≠0 , and iii) damage severity level ≠ No Damage & Δ≠0 (i.e. the intersection of the first two samples).

Damage Severity Level					
Construction Material	**D1**	**D2**	**D3**	**D4**	**Total number**
Masonry (nr. 528)	23	113	158	73	367
Reinforced concrete (nr.57)	3	8	6	3	20
Stones (nr.15)	0	2	3	2	7
Differential Displacement					
Construction Material	**Δ < 3 mm**	**3 < Δ < 5 mm**	**5 < Δ < 10 mm**	**Δ > 10 mm**	**Total number**
Masonry (nr. 528)	91	91	138	72	392
Reinforced concrete (nr.57)	13	8	14	13	48
Stones (nr.15)	0	1	8	0	9
Damage Severity Level of buildings with Δ≠0					
Construction Material	**D1**	**D2**	**D3**	**D4**	**Total number**
Masonry (nr. 528)	14	69	120	72	275
Reinforced concrete (nr.57)	3	4	5	3	15
Stones (nr.15)	0	0	0	2	2

The correlations between damage severity and the *Subsidence-Related Intensity* (SRI) parameters, i.e. differential settlements (Δ) and relative rotation (θ) were then obtained for the samples of 275 masonry (Fig. 12) and 15 reinforced concrete buildings (Fig.13). For both building categories and SRI, as expected, it is observed that when the SRI increases the damage level increases accordingly. Moreover, the empirical fragility curves generated respectively for Δ and θ give a probabilistic representation of damage occurrence according to a given severity level.

With reference to the analysed sample of 275 masonry buildings in Como historic city centre (Fig. 12c and d), damage levels affecting the aesthetic of building façades as D1 (w < 0.1 mm) and D2 (w < 1 mm) appear totally reached for Δ = 15 mm or θ = 0.5E-03 rad and Δ = 17 mm or θ = 0.6E-03 rad, respectively. Slight damage D3 (w < 5mm) is reached at Δ = 20 mm or θ = 0.7E-03 rad, while D4 (w > 5 mm) at Δ = 25 mm or θ = 1.0E-03 rad. Importantly, both SRI parameters have similar trends with low Coefficients of Variation (CV = σ/μ) that can be associated with high precision. This is in agreement with studies available in literature, where similar approaches were used over larger samples of buildings [e.g. 15]. Moreover, both Δ and θ have low PCC values ($PCC = Covariance_{(damage\ level,SRI)}/\sigma_{damage\ level} \cdot \sigma_{SRI}$) describing weak or null linear correlations with damage levels, due to the high dispersion of sampling data. In Figure 12 fragility parameters (β and $\overline{\mathrm{SRI}}$) are shown with reference to both SRI for masonry buildings.

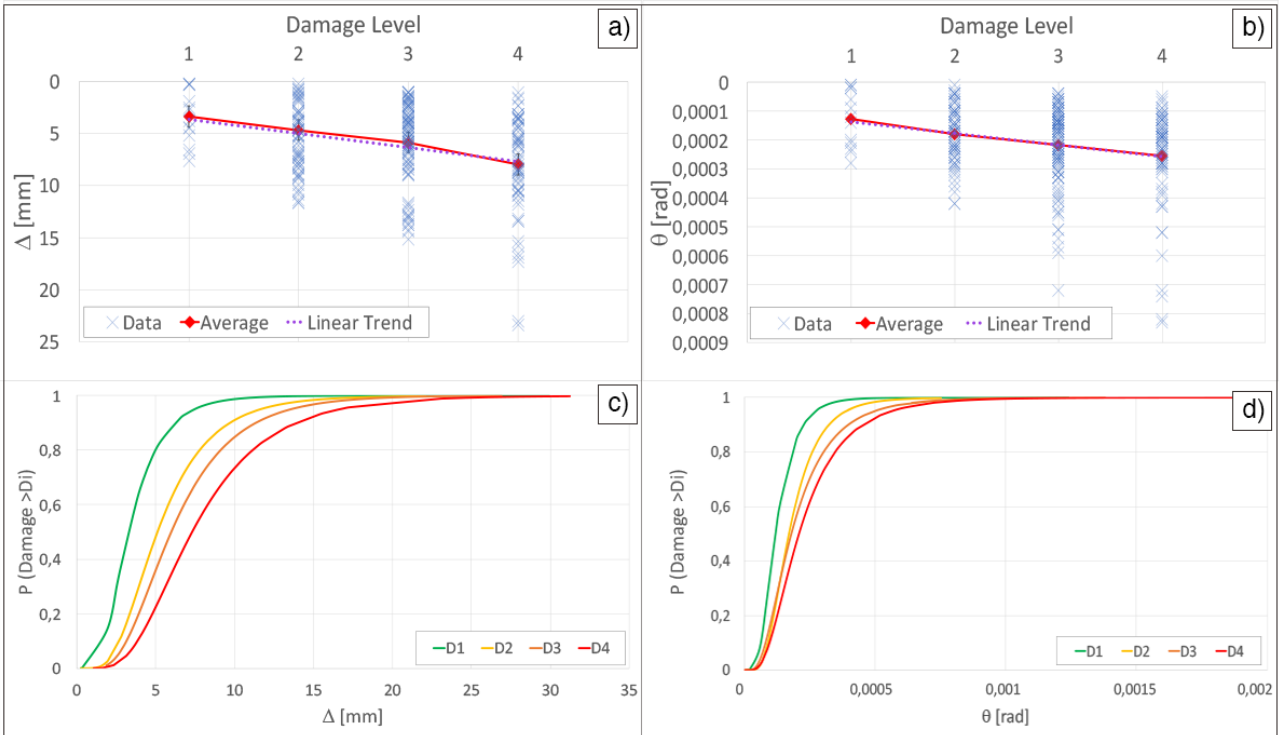

Damage Level	Average Δ [mm]	Std.Dev. (σ)[mm]	Median ($\bar{\Delta}$)[mm]	β [mm]	CV
D1	3.38	2.60	3.27	1.32	0.77
D2	4.67	3.18	5.10	0.83	0.68
D3	6.61	3.83	6.00	0.71	0.58
D4	7.97	4.67	7.31	0.62	0.59
PCC = 0.28					

Damage Level	Average θ [rad]	Std.Dev. (σ) [rad]	Median ($\bar{\theta}$)[rad]	β [rad]	CV
D1	0.13E-03	9.80E-05	0.12E-03	1.25	0.75
D2	0.18E-03	9.93E-05	0.17E-03	0.73	0.55
D3	0.22E-03	0.13E-03	0.18E-03	0.62	0.59
D4	0.26E-03	0.17E-03	0.21E-03	0.58	0.65
PCC = 0.16					

Figure 12. Results for buildings of masonry type (nr.275). Damage level vs a) differential settlements (Δ) and b) relative rotation (θ). Fragility curves and parameters of log normal distribution function for c) differential settlements (Δ) and d) relative rotation (θ).

Despite the limited number of buildings (i.e. 15), similar results were obtained also for the reinforced concrete buildings (Fig. 13). In this case, aesthetic damage D1 (w < 0.1 mm) and D2 (w < 1 mm) appear totally reached for Δ = 7 mm or θ = 0.3E-03 rad and Δ = 20 mm or θ = 0.6E-03 rad, respectively. Moderate damage D3 (w < 5mm) is reached at Δ = 22 mm or θ = 0.8E-03 rad, whereas D4 (w > 5 mm) at Δ = 40 mm or θ = 1.3E-03 rad. The Coefficients of Variation (CV = σ/μ) obtained for reinforced concrete buildings are lower than those for masonry buildings, thus suggesting a higher precision and an easier way to link a given SRI to distinct damage levels. Moreover, the PCC shows here strong and moderately strong linear correlations of Δ and θ with the damage severity levels. Figure 13 shows the fragility parameters (β and $\overline{\text{SRI}}$) of both SRI for reinforced concrete buildings.

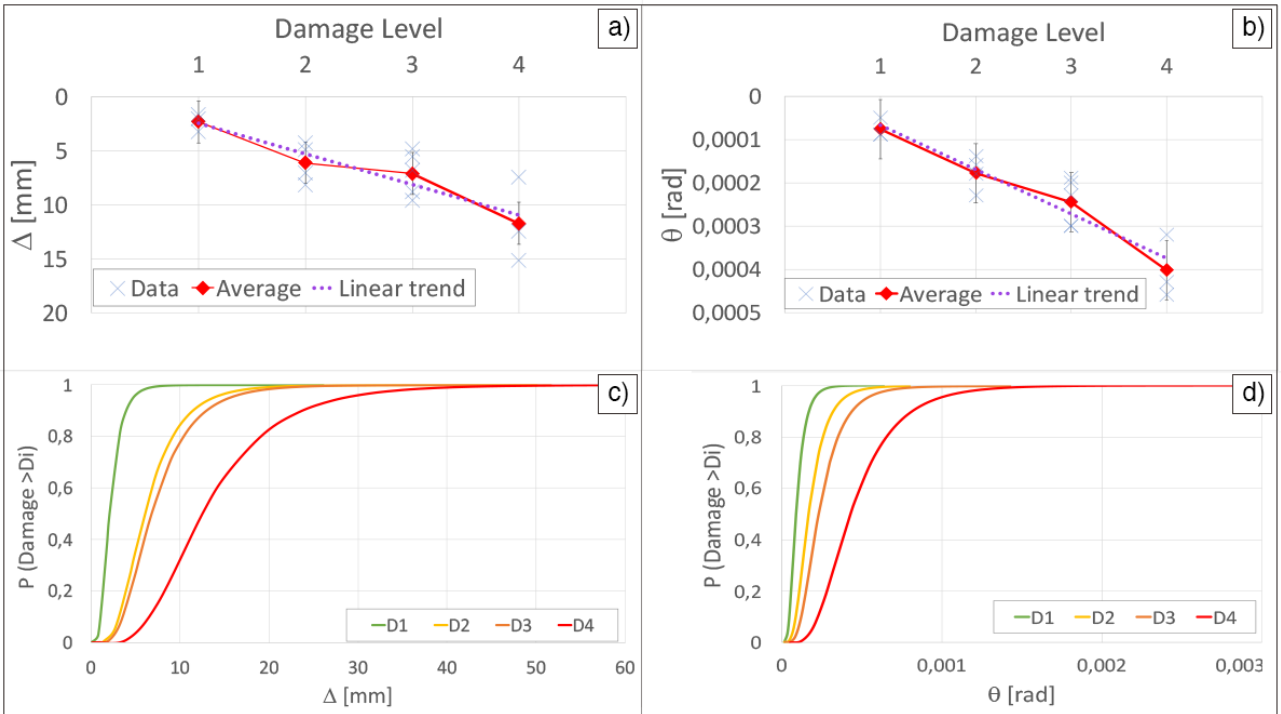

Damage Level	Average Δ [mm]	Std.Dev. (σ) [mm]	Median ($\bar{\Delta}$) [mm]	β [mm]	CV
D1	2.34	0.80	2.07	0.33	0.34
D2	6.14	1.81	6.03	0.30	0.29
D3	7.15	2.04	6.84	0.29	0.28
D4	11.73	3.93	12.51	0.37	0.33
PCC = 0.80					

Damage Level	Average θ [rad]	Std.Dev. (σ) [rad]	Median ($\bar{\theta}$) [rad]	β [rad]	CV
D1	7.67E-05	2.31E-05	0.09E-03	0.34	0.30
D2	0.18E-03	3.86E-05	0.17E-03	0.21	0.21
D3	0.24E-03	5.32E-03	0.23E-03	0.22	0.22
D4	0.40E-03	7.37E-03	0.43E-03	0.19	0.18
PCC = 0.51					

Figure 13. Results for reinforced concrete buildings (nr.15). Damage level vs a) differential settlements (Δ) and b) relative rotation (θ). Fragility curves and parameters of log normal distribution function for c) differential settlements (Δ) and d) relative rotation (θ).

5. Discussion

Como historic centre has experienced continuous lowering of the ground surface due to both natural and anthropogenic causes since 1945-1950. The presence of highly compressible Holocene stratigraphic units and the piezometric level variations have been proved to be the main drivers of subsidence in Como basin [54-57]. The lakefront area and the western sector of Como historic centre, although having different hydrogeological and stratigraphic properties, showed the largest InSAR-derived vertical displacements, i.e. more than 25 mm in 9 years, following the pre-Roman Lake Como shoreline (dated about I century BC). In its current setting, Como costal area is the result of anthropogenic modifications started in Roman age with the city founding (59 BC), and continued with the progressive filling of the lakefront area and urbanization, the exploitation of deep aquifer in 1950-1975, up to the recent construction of antiflooding facilities in 2008-2010 [54,56]. In this first analysis, the interplay between subsoil and single-building foundation could not be taken into consideration when interpreting the InSAR data because of i) the dense urbanised area with average distance between buildings of 5 m, and ii) the InSAR spatial resolution of about 10 m. Although this hampered the distinction between the settlements in “free field” conditions from those on top of the buildings, the spatial pattern of vertical displacements is in agreement with those obtained by Nappo et al. [57] for the entire basin of Como. Indeed, the hydrogeological features of Como historic centre

have been assumed invariant in both 1992-2010 [57] and 2010-2019 time ranges because the study area is densely urbanised and this would allow only confined anthropic modifications that may hardly interfere with the stratigraphy of the subsoil [57]. As for the piezometric level, this is proved to have seasonal fluctuations [54-56] that can be considered negligible in the investigated time frame. However, new and detailed piezometric measurements and investigations might help in determining the specific relationship between the local hydrogeological and stratigraphic setting and InSAR-derived ground surface displacements. Further deepening is also necessary towards the integration of the piezometric and lake level variations to determine their influence on the measured settlements at the city scale.

The majority of buildings in Como historic centre shows moderate (D3) or low (D2) damage. This depends on the conservation status of each building and the frequency of maintenance/restoration works that may bias the crack pattern evolution on building façades. As a result, this can induce overestimations or underestimations of the damage status of some buildings, especially those with very low damage (D1), and therefore affect the vulnerability analysis. Furthermore, the classification of building damage, although derived from the measurement of cracks width, is still qualitative and based only on exterior evidence of cracks. Moreover, although buildings in subsiding areas can experience sagging that induces cracks wider at the top and narrow at the bottom, or hogging with cracks tinier at the top and wider at the bottom [5] in this work the damage was assumed to be caused only by vertical movements without considering possible tilting. Future works may, therefore, concern a more comprehensive assessment of building damage status by i) combining exterior and interior cracks surveys, and ii) considering movements in both vertical and horizontal directions, by using for instance a combination of InSAR data in ascending and descending orbits. Importantly, the distribution of PT within the building footprint should also be taken into account in this type of analysis. Indeed, sparse rather than concentrated PT could better describe the performance of the building as a whole.
In addition, the typology of foundations determines the response of the buildings to ground differential displacements or relative rotations, thus resulting in different crack patterns on the façades. In this work, we had no information about building foundations, and therefore intrinsically assumed a unique typology, i.e. shallow foundations.

Importantly, the observation period of InSAR dataset (9 years) seems rather limited with respect to the time range in which building settlements may have cumulated (see for instance the abovementioned studies on subsidence) thus resulting in damage to structures. This is a typical limitation to this kind of analyses, when only a single damage survey is available (see for instance Peduto et al. [15]). However, in this study the considered period can reasonably approximate the frequency of restoration works to façades in Como historic centre, where high attention to building health is continuously paid.

As for the results of the vulnerability analysis shown in Figures 12 and 13, unluckily there are still few examples in literature dealing with extensive studies involving masonry and reinforced concrete buildings resting on shallow foundations in subsiding areas [e.g. 9,15]. For instance, the qualitative comparison of average values, standard deviations and fragility curves obtained here and by Peduto et al. [15] for four municipalities in The Netherlands highlighted differences in both the differential settlements (Δ) and relative rotations (θ) due to diverse procedures adopted for their computation. In

particular, here the length (L) is calculated as the Euclidean distance between $\delta_{v,max}$ and $\delta_{v,min}$, rather than from the profile plotting of InSAR data interpolated within each building [15]. Further differences may be related to i) the typology of analysed buildings (e.g. 2-3 floors in The Netherlands and up to 6 floors in Como), ii) the foundation system (official sources allowed the selection of buildings on shallow foundations in The Netherlands), and iii) different finishing of the façades (with plaster in Como and without plaster in The Netherlands). The combined effect of these factors may have influenced the cracks onset and development.

6. Conclusions

This paper analysed the effects (in terms of damage) on buildings of the well-known subsidence phenomenon that affects the historic centre of Como municipality using subsoil hydrogeological features, in situ damage investigations dated 2019, and CSK X-band InSAR measurements from 2010 to 2019. First, the correlation between subsidence predisposing factors and ground surface displacements were qualitatively assessed to determine the influence of local subsoil features on the observed InSAR signal in the investigated period. Although needing further investigations, the results highlighted that the largest InSAR-derived vertical displacements occur in the area occupied by Lake Como during the pre-Roman period; the same area is nowadays urbanised.

Six-hundred buildings of the city centre were surveyed, and those showing not-negligible damage and differential settlements (i.e. 275 of masonry type and 15 of reinforced concrete) were selected to perform the vulnerability analysis of Como city centre. Regardless of the limitations mentioned in the Discussion, using empirical fragility curves the probability of occurrence of a certain damage level was derived when a building is subjected to differential settlements and relative rotations of given intensity. As expected, the relationship between causes (subsidence intensity) and effects (damage severity level) showed that the most severe damage occurs where buildings experience higher differential displacements or relative rotations. From the comparison of these two parameters, the differential settlements allowed a better distinction between damage severity levels. This is therefore the parameter to be preferred in future analyses at the municipal scale encompassing more buildings of Como historic centre. In this perspective, when further information about building/foundation characteristics and maintenance works become available, it will be integrated with the current preliminary results to derive a more accurate vulnerability analysis of Como historic centre.

Finally, the fragility curves as resulted from this work highlighted that i) such probabilistic analyses should involve a broader sample of data in order to be more reliable and to better account for inherent variability of the building/soil features; ii) fragility curves should be performed with reference to a specific type of building (e.g., construction material, geometry, age), foundation system (e.g., shallow, piled, etc.), and interacting subsoil, and iii) damage acceptable in one region or for a given type of building might be unacceptable elsewhere (in agreement with Burland et al. [4]).

Therefore, future works are intended to extend the present results to the entire Como municipality, and to develop forecasting models of damage occurrence on historical buildings for risk management purposes.

Acknowledgements

Project carried out using CSK® Products, © ASI (Italian Space Agency), delivered under an ASI licence to use. The authors would also like to acknowledge the Editor and five anonymous reviewers for their valuable suggestions that helped improving the current version of the paper.

References

[1] Bjerrum, L., 1963. Allowable settlement of structures. 3rd European Conference on Soil Mechanics and Foundation ENgineering, Wiesbaden, 2, Brighton, England, 135–137.

[2] Bjerrum, L., 1967. Engineering geology of Norwegian normally-consolidated marine clays as related to settlements of buildings. Geotechnique, 17: 81-118.

[3] Boscardin, M.D., Cording, E.G., 1989. Building response to excavation induced settlement. J. Geotech. Eng. 115, 1-21

[4] Burland, J. B., Broms, B. B., De Mello, V. F. B., 1977. Behaviour of Foundations and Structures Comportement des Fondations et des Structures. State of the Art Report, 363–400. https://inspectapedia.com/structure/Behaviour-of-Foundations-Footings-Burland.pdf

[5] Burland, J. B., Wroth, C. P., 1974. Settlement of buildings and associated damage. Settlement of Structures, Proceedings of the Conference of the British Geotechnical Society, 611–764. https://www.researchgate.net/publication/248646701

[6] Skempton, A. W., MacDonald, D. H., 1956. The allowable settlements of buildings. Proceedings of the Institution of Civil Engineers. https://doi.org/10.1680/ipeds.1956.12202

[7] Timoshenko, S., 1957. Strength of material-part I. D. van No- strand Co, London.

[8] Saeidi, A., Deck, O., Verdel, T., 2013. Comparison of Building Damage Assessment Methods for Risk Analysis in Mining Subsidence Regions. Geotechnical and Geological Engineering, 31(4), 1073–1088. https://doi.org/10.1007/s10706-013-9633-7

[9] Zhang, L., Ng, A. M. Y., 2005. Probabilistic limiting tolerable displacements for serviceability limit state design of foundations. Geotechnique, 55(2), 151–161. https://doi.org/10.1680/geot.2005.55.2.151

[10] Peduto, D., Ferlisi, S., Nicodemo, G., Reale, D., Pisciotta, G., Gullà, G., 2017. Empirical fragility and vulnerability curves for buildings exposed to slow-moving landslides at medium and large scales. Landslides, 14(6), 1993–2007. https://doi.org/10.1007/s10346-017-0826-7

[11] Peduto, D., Nicodemo, G., Maccabiani, J., Ferlisi, S., 2017b. Multi-scale analysis of settlement-induced building damage using damage surveys and DInSAR data: A case study in The Netherlands. Engineering Geology, 218, 117–133. https://doi.org/10.1016/j.enggeo.2016.12.018

[12] Saeidi, A., Deck, O., Verdel, T., 2009. Development of building vulnerability functions in subsidence regions from empirical methods. Engineering Structures, 31(10), 2275–2286. https://doi.org/10.1016/j.engstruct.2009.04.010

[13] Ferlisi, S., Nicodemo, G., Peduto, D., Negulescu, C., Grandjean, G., 2019. Deterministic and probabilistic analyses of the 3D response of masonry buildings to imposed settlement troughs, Georisk: Assessment and Management of Risk for Engineered Systems and Geohazards, DOI: 10.1080/17499518.2019.1658880

[14] Béjar-Pizarro, M., Guardiola-Albert, C., García-Cárdenas, R. P., Herrera, G., Barra, A., Molina, A. L., Tessitore, S., Staller, A., Ortega-Becerril, J. A., García-García, R. P., 2016. Interpolation of GPS and geological data using InSAR deformation maps: Method and application to land subsidence in the alto guadalentín aquifer (SE Spain). Remote Sensing, 8(11). https://doi.org/10.3390/rs8110965

[15] Peduto, D., Korff, M., Nicodemo, G., Marchese, A., Ferlisi, S., 2019. Empirical fragility curves for settlement-affected buildings: Analysis of different intensity parameters for seven hundred masonry buildings in The Netherlands. Soils and Foundations, 59(2), 380–397. https://doi.org/10.1016/j.sandf.2018.12.009

[16] Ezquerro, P., Del Soldato, M., Solari, L., Tomàs, R., Raspini, F., Ceccatelli, M., Fernàndez-Merodo, J.A., Casagli, N., Herrera, G., 2020. Vulnerability Assessment of Buildings due to Land Subsidence using InSAR Data in the Ancient Historical City of Pistoia (Italy). Sensors (Basel). 2020;20(10):E2749. Published 2020 May 12. doi:10.3390/s20102749

[17] Mavrouli, O., Fotopoulou, S., Pitilakis, K., Zuccaro, G., Corominas, J., Santo, A., Cacace, F., De Gregorio, D., Di Crescenzo, G., Foerster, E., Ulrich, T., 2014. Vulnerability assessment for reinforced concrete buildings exposed to landslides. Bulletin of Engineering Geology and the Environment, 73(2), 265–289. https://doi.org/10.1007/s10064-014-0573-0

[18] Negulescu, C., Ulrich, T., Baills, A., Seyedi, D. M., 2014. Fragility curves for masonry structures submitted to permanent ground displacements and earthquakes. Natural Hazards, 74(3), 1461–1474. https://doi.org/10.1007/s11069-014-1253-x

[19] Wiebe, D., Cox, D., 2014. Application of fragility curves to estimate building damage and economic loss at a community scale: A case study of Seaside, Oregon. Nat. Hazards 2014, 71, 2043–2061. doi:10.1007/s11069- 013-0995-1

[20] Solari, L., Del Soldato, M., Bianchini, S., Ciampalini, A., Ezquerro, P., Montalti, R., Raspini, F., Moretti, S., 2018. From ERS 1/2 to Sentinel-1: Subsidence Monitoring in Italy in the Last Two Decades. Frontiers in Earth Science, 6(October), 1–16. https://doi.org/10.3389/feart.2018.00149

[21] Gee, D., Sowter, A., Grebby, S., de Lange, G., Athabb, A., Marsha, S., 2019. National geohazards mapping in Europe: interferometric analysis in The Netherlands. Engineering Geology, 256, 1-22.

[22] Peduto, D., Cascini, L., Arena, L., Ferlisi, S., Fornaro, G., Reale, D., 2015. A general framework and related procedures for multiscale analyses of DInSAR data in subsiding urban areas. ISPRS Journal of Photogrammetry and Remote Sensing, 105, 186–210. https://doi.org/10.1016/j.isprsjprs.2015.04.001

[23] Berardino, P., Fornaro, G., Lanari, R., Sansosti, E., 2002. A new algorithm for surface deformation monitoring based on small baseline differential SAR interferograms. IEEE Transactions on Geoscience and Remote Sensing, 40(11), 2375–2383. https://doi.org/10.1109/TGRS.2002.803792

[24] Crosetto, M., Monserrat, O., Cuevas-González, M., Devanthéry, N., Crippa, B., 2016. Persistent Scatterer Interferometry: A review. ISPRS Journal of Photogrammetry and Remote Sensing, 115, 78–89. https://doi.org/10.1016/j.isprsjprs.2015.10.011

[25] Crosetto, M., Solari, L., Mróz, M., Balasis-Levinsen, J., Casagli, N., Frei, M., Oyen, A., Moldestad, D.A., Bateson, L., Guerrieri, L., Comerci, V., Andersen, H.S., 2020, The Evolution of Wide-Area DInSAR: From Regionaland National Services to the European GroundMotion Service. Remote Sens.,12, 2043; doi:10.3390/rs12122043

[26] Ferretti, A., Prati, C., Rocca, F., 2001. Permanent scatterers in SAR interferometry. IEEE Transactions on Geoscience and Remote Sensing, 39(1), 8–20. https://doi.org/10.1109/36.898661

[27] Ferretti, A., Fumagalli, A., Novali, F., Prati, C., Rocca, F., Rucci, A., 2011. A new algorithm for processing interferometric data-stacks: SqueeSAR. IEEE Transactions on Geoscience and Remote Sensing, 49(9), 3460–3470. https://doi.org/10.1109/TGRS.2011.2124465

[28] Hooper, A., Zebker, H., Segall, P., Kampes, B., 2004. A new method for measuring deformation on volcanoes and other natural terrains using InSAR persistent scatterers. Geophysical Research Letters, 31(23), 1–5. https://doi.org/10.1029/2004GL021737

[29] Hooper, A. J., 2008. A multi-temporal InSAR method incorporating both persistent scatterer and small baseline approaches. Geophysical Research Letters, 35(16), 1–5. https://doi.org/10.1029/2008GL034654

[30] Hooper, A., Bekaert, D., Spaans, K., Arikan, M., 2012. Recent advances in SAR interferometry time series analysis for measuring crustal deformation. Tectonophysics, 514–517, 1–13. https://doi.org/10.1016/j.tecto.2011.10.013

[31] Monserrat, O., Crosetto, M., Luzi, G., 2014. A review of ground-based SAR interferometry for deformation measurement. ISPRS Journal of Photogrammetry and Remote Sensing, 93, 40–48. https://doi.org/10.1016/j.isprsjprs.2014.04.001

[32] Wasowski, J., Bovenga, F., 2014. Investigating landslides and unstable slopes with satellite Multi Temporal Interferometry: Current issues and future perspectives. Engineering Geology, 174, pp. 103-138.

[33] Baldi, P., Casula, G., Cenni, N., Loddo, F., Pesci, A., 2009. GPS-based monitoring of land subsidence in the Po Plain (Northern Italy). Earth and Planetary Science Letters, 288(1–2), 204–212. https://doi.org/10.1016/j.epsl.2009.09.023

[34] Bozzano, F., Esposito, C., Mazzanti, P., Patti, M., Scancella, S., 2018. Imaging multi-age construction settlement behaviour by advanced SAR interferometry. Remote Sensing, 10(7). https://doi.org/10.3390/rs10071137

[35] Bru, G., Herrera, G., Tomás, R., Duro, J., de la Vega, R., Mulas, J., 2013. Control of deformation of buildings affected by subsidence using persistent scatterer interferometry. Structure and Infrastructure Engineering, 9(2), 188–200. https://doi.org/10.1080/15732479.2010.519710

[36] Brunori, C.A., Bignami, C., Albano, A., Zucca, F., Samsonov, S., Groppelli, G., Norini, G., Saroli, M., Stramondo, S., 2015. Land subsidence, Ground Fissures and Buried Faults: InSAR Monitoring of Ciudad Guzmán (Jalisco, Mexico). Remote Sens., 7(7), 8610-8630; https://doi.org/10.3390/rs70708610

[37] Cascini, L., Peduto, D., Reale, D., Arena, L., Ferlisi, S., Verde, S., Fornaro, G., 2013. Detection and monitoring of facilities exposed to subsidence phenomena via past and current generation SAR sensors. Journal of Geophysics and Engineering, 10(6). https://doi.org/10.1088/1742-2132/10/6/064001

[38] Cigna, F., Osmanoğlu, B., Cabral-Cano, E., Dixon, T. H., Ávila-Olivera, J. A., Garduño-Monroy, V. H., DeMets, C., Wdowinski, S., 2012. Monitoring land subsidence and its induced geological hazard with Synthetic Aperture Radar Interferometry: A case study in Morelia, Mexico. Remote Sensing of Environment, 117, 146–161. https://doi.org/10.1016/j.rse.2011.09.005

[39] Del Ventisette, C., Solari, L., Raspini, F., Ciampalini, A., di Traglia, F., Moscatelli, M., Pagliaroli, A., Moretti, S., 2015. Use of PSInSAR data to map highly compressible soil layers. Geologica Acta, 13(4), 309–323. https://doi.org/10.1344/GeologicaActa2015.13.4.4

[40] Del Soldato, Matteo; Farolfi, Gregorio; Rosi, Ascanio; Raspini, Federico; Casagli, Nicola. 2018. "Subsidence Evolution of the Firenze–Prato–Pistoia Plain (Central Italy) Combining PSI and GNSS Data" *Remote Sens.* 10, no. 7: 1146.

[41] Farolfi, G., Del Soldato, M., Bianchini, S., Casagli, N., 2019. A procedure to use GNSS data to calibrate satellite PSI data for the study of subsidence:an example from the north-western Adriatic coast (Italy). European Journal of Remote Sensing, 52(sup4), 54–63. https://doi.org/10.1080/22797254.2019.1663710

[42] Herrera, G., Fernández, J. A., Tomás, R., Cooksley, G., Mulas, J., 2009. Advanced interpretation of subsidence in Murcia (SE Spain) using A-DInSAR data - Modelling and validation. Natural Hazards and Earth System Science, 9(3), 647–661. https://doi.org/10.5194/nhess-9-647-2009

[43] Herrera, G., Tomás, R., Monells, D., Centolanza, G., Mallorquí, J. J., Vicente, F., Navarro, V. D., Lopez-Sanchez, J. M., Sanabria, M., Cano, M., Mulas, J., 2010. Analysis of subsidence using TerraSAR-X data: Murcia case study. Engineering Geology, 116(3–4), 284–295. https://doi.org/10.1016/j.enggeo.2010.09.010

[44] Hu, B., Chen, J., Zhang, X., 2019. Monitoring the land subsidence area in a coastal urban area with InSAR and GNSS. Sensors (Switzerland). https://doi.org/10.3390/s19143181

[45] Karila, K., Karjalainen, M., Hyyppä, J., Koskinen, J., Saaranen, V., Rouhiainen, P., 2013. A comparison of precise leveling and Persistent Scatterer SAR Interferometry for building subsidence rate measurement. ISPRS International Journal of Geo-Information. https://doi.org/10.3390/ijgi2030797

[46] Peduto, D., Giangreco, C., Venmans, A. A.M., 2020. Differential settlements affecting transition zones between bridges and road embankments on soft soils: Numerical analysis of maintenance scenarios by multi-source monitoring data assimilation, Transportation Geotechnics, Volume 24, ISSN 2214-3912, https://doi.org/10.1016/j.trgeo.2020.100369.

[47] Polcari, M., Albano, M., Saroli, M., Tolomei, C., Lancia, M., Moro, M., Stramondo, S., 2014. Subsidence Detected by Multi-Pass Differential SAR Interferometry in the Cassino Plain (Central Italy): Joint Effect of Geological and Anthropogenic Factors?. Remote Sensing, 6(10), 9676-9690;

https://doi.org/10.3390/rs6109676

[48] Polcari, M., Moro, M., Romaniello, V., Stramondo S., 2019. Anthropogenic subsidence along railway and road infrastructures in Northern Italy highlighted by Cosmo-SkyMed satellite data. Journal of Applied Remote Sensing 13(2).

[49] Sanabria, M.P., Guardiola-Albert, C., Tomas, R., Herrera, G., Prieto, A., Sanchez, H., Tessitore, S., 2014. Subsidence activity maps derived from DInSAR data: Orihuela case study. Nat. Hazards Earth Syst. Sci. 14, 1341-1360

[50] Solari, L., Ciampalini, A., Raspini, F., Bianchini, S., Moretti, S., 2016. PSInSAR analysis in the pisa urban area (Italy): A case study of subsidence related to stratigraphical factors and urbanization. Remote Sensing, 8(2). https://doi.org/10.3390/rs8020120

[51] Stramondo, S, Saroli, M., Tolomei, C., Moro, M., Doumaz, F., Pesci, A., Loddo, F., Baldi, P., Boschi, E., 2007. Surface movements in Bologna (Po Plain — Italy) detected by multitemporal DInSAR. Remote Sensing of Environment, 110 (3), 304-316. https://doi.org/10.1016/j.rse.2007.02.023.

[52] Stramondo, S., Bozzano, F., Marra, F., Wegmuller, U., Cinti, F. R., Moro, M., Saroli, M., 2008. Subsidence induced by urbanisation in the city of Rome detected by advanced InSAR technique and geotechnical investigations. Remote Sensing of Environment, 112(6), 3160–3172. https://doi.org/10.1016/j.rse.2008.03.008

[53] Tosi, L., Teatini, P., Carbognin, L., Brancolini, G., 2009. Using high resolution data to reveal depth-dependent mechanisms that drive land subsidence: The Venice coast, Italy. Tectonophysics, 474(1–2), 271–284. https://doi.org/10.1016/j.tecto.2009.02.026

[54] Bajni, G., Apuani, T., Beretta, G. P., 2019. Hydro-geotechnical modelling of subsidence in the Como urban area. Engineering Geology, 257(September 2018), 105144. https://doi.org/10.1016/j.enggeo.2019.105144

[55] Comerci, V., Capelletti, S., Michetti, A. M., Rossi, S., Serva, L., Vittori, E., 2007. Land subsidence and Late Glacial environmental evolution of the Como urban area (Northern Italy). Quaternary International, 173–174(SUPPL.), 67–86. https://doi.org/10.1016/j.quaint.2007.06.014

[56] Ferrario, M. F., Bonadeo, L., Brunamonte, F., Livio, F., Martinelli, E., Michetti, A. M., Censi Neri, P., Chiessi, V., Comerci, V., Höbig, N., 2015. Late Quaternary environmental evolution of the Como urban area (Northern Italy): A multidisciplinary tool for risk management and urban planning. Engineering Geology, 193, 384–401. https://doi.org/10.1016/j.enggeo.2015.05.013

[57] Nappo, N., Ferrario, M.F., Livio, F., Michetti, A.M., 2020. Regression analysis of subsidence in Como basin (northern Italy): new insights on natural and anthropic drivers from InSAR data. Remote Sensing 12, 2931.

[58] Comune di Como, 1980. Relazione di sintesi della Commissione per lo Studio dei Fenomeni di Subsidenza. Documenti e Ricerche 34.

[59] Bini, A., 1987. L'apparato glaciale wurmiano di Como. Unpublished Ph. D. thesis, University of Milan, Italy.

[60] Bini, A., 1993. Geologia del Quaternario e geomorfologia della Piana di Como. In: Uboldi, M. (Ed.), Carta archeologica della Lombardia vol. III. Franco Cosimo Panini, pp. 59–63.

[61] Bini, A., 1996. La regolazione del Lago di Como: problemi e proposte. Atti del convegno. Villa Olmo, Como, 19 April 1996. Kiwanis International Europe.

[62] Bini, A., Castelletti, L., 1986. Geologia e paleobotanica di un sedimento olocenico nel sottosuolo di piazza Roma a Como. Nat. Bresciana 23, 357–363.

[63] Castelletti, L., Orombelli, G., 1986. Una nuova data 14C per la storia della deglaciazione del bacino del Lago di Como. Geogr. Fis. Din. Quat. 9, 56–58

[64] Beretta, G.P., Denti, E., Fumagalli, L., Sala, P., 1986. Note sull'idrogeologia delle città di Como e Lecco. Mem. Soc. Geol. Ital. 32 (1986), 235–251.

[65] Apuani, T., Cancelli, A., Cancelli, P., 2000. Hydrogeological and geotechnical investigations along the shoreline of the town of Como, Italy. In: Moore, D.P., Hungr, O. (Eds.), “Engineering Geology and

Environment" Proc. 8th. Cong. Intern. Assoc. Engineering Geology.

[66] Caniggia, G., 1968. Lettura di una città: Como. p. 46.

[67] Ferrario M.F., Brunamonte F., Caccia A., Livio F., Martinelli E., Mazzola E., Michetti A.M., Terrana S., 2015. Buried Landscapes: Geoarchaeology of the Roman Harbor of Como (N Italy), Alpine and Mediterranean Quaternary, 28 (2), 111 – 120, ISSN (online): 2279-7335

[68] Luraschi, G., 1987. Como romana: le mura. Como nell'antichità. Soc. Arch. Com., pp. 103–112.

[69] Uboldi, M., 1993. Carta archeologica della Lombardia. In: Franco Cosimo Panini, Como. La città murata e la convalle.

[70] Sileo G., Giardina F., Livio F., Michetti A.M., Mueller K., Vittori E., 2007. Remarks on the Quaternary tectonics of the Insubria Region (Lombardia North Western Italy, and Ticino, South Eastern Swizerland). Boll. Soc. Geol. It. - Italian Journal of Geoscience 126(2), 411-425, ISSN: 0037-8763

[71] Livio, F., Berlusconi, A., Chunga, K., Michetti, A. M., Sileo, G., 2011. New stratigraphic and structural evidence for Late Pleistocene surface faulting along the Monte Olimpino Backthrust (Lombardia, N Italy). Online Soc. Geol. It, 14, 17-25.

[72] Michetti, A.M., Giardina, F., Livio, F., Mueller, K., Serva, L., Sileo, G., Rogledi, S., 2012. Active compressional tectonics, Quaternary capable faults, and the seismic landscape of the Po Plain (N Italy). Annals of Geophysics.

[73] Comerci, V., 2004. Evoluzione geologica e ambientale recente in aree subsidenti, esempio di studio nella città di Como. Università degli Studi dell'Insubria (Ph.D. Thesis).

[74] Martinelli, E., Castelletti, L., Ferrario, M. F., Livio, F., Michetti, A. M., 2019. Archeologia e indagini stratigrafiche per la ricostruzione della linea di costa e delle aree portuali della Como romana. Rivista archeologica dell'antica provincia e diocesi di Como, vol.200.

[75] Bernoulli, D., Bertotti, G., Zingg, A., 1989. Northward thrusting of the Gonfolite Lombarda («South-Alpine Molasse») onto the Mesozoic sequence of the Lombardian Alps; implications for the deformation history of the Southern Alps. Ecl. Geol. Helv., 82(3), 841-856.

[76] Michetti, A.M., Livio, F., Pasquaré, F.A., Vezzoli, L., Bini, A., Bernoulli, D., Sciunnach, D., 2014. Note Illustrative della Carta Geologica d'Italia, Foglio 075, Como, Progetto CARG, 206 p., http://www.isprambiente.gov.it/Media/carg/note_illustrative/75_Como.pdf

[77] Rossi, S., Alberti, F., Felber, M., Bini, A., 1991. Evidenze di fluttuazioni glaciali würmiane nella bassa valle della Breggia (Cernobbio, Como). Bollettino della Società Ticinese di Scienze Naturali LXXIX, 25-47.

[78] SERVIZIO GEOLOGICO D'ITALIA, 2015– Carta Geologica d'Italia alla scala 1:50000 – Foglio n. 75 "Como".

[79] Wegmuller, U., Werner, C., 1997. Gamma SAR processor and interferometry software. In Proceedings of the ERS Symposium on Space at the Service of Our Environment, Florence, Italy, 14–21 March 1997; ESA Publications Division: Florence, Italy, 1997; pp. 1687–1692.

[80] Werner, C., Wegmüller, U., Strozzi, T., Wiesmann, A., 2003. Interferometric Point Target Analysis for Deformation Mapping. International Geoscience and Remote Sensing Symposium (IGARSS), 7, 4362–4364. https://doi.org/10.1109/igarss.2003.1295516

[81] Goldstein, R., Werner, C., 1998. "Radar interferogram filtering for geophysical applications," Geophys. Res. Lett. 25, 4035–4038.

[82] Costantini, M., 1998. A novel phase unwrapping method based on network programming. IEEE Trans. Geosci. Remote Sens. 36, 813–821.

[83] Carta Tecnica Regional – CTR Lombardia. Geoportale Regione Lombardia. Available online: http://www.geoportale.regione.lombardia.it/ - last access June 2020.

[84] SiT, 2020. https://www.comune.como.it/it/servizi/urbanistica/sit/ - Last access: June 2020.

[85] Krivoruchko, K., 2012. Empirical Bayesian Kriging; Esri: Redlands, CA, USA.

[86] Wackernagel, H. 1995. Ordinary Kriging. In Multivariate Geostatistics; Springer: Berlin/Heidelberg, Germany, pp.74-81.